Aus dem Institut für Lasermedizin
Direktor: Prof. Dr. Peter Hering

Holographic topometry with high resolution for forensic facial reconstruction

D I S S E R T A T I O N

zur Erlangung des Grades eines Doktors der
Zahnmedizin

Der Medizinischen Fakultät der Heinrich-Heine-Universität
Düsseldorf

vorgelegt von

Frank Prieels

Dezember 2009

Contents

1 Introduction **2**

2 The human face **3**

2.1 Importance of the face . . . 3
2.2 Facial Recognition . . . 3
2.3 Facial Structure . . . 4
2.3.1 Skull . . . 4
2.3.2 Soft Tissue . . . 8

3 Facial Reconstruction **11**

3.1 History - overview . . . 11
3.2 Soft tissue measurement . . . 17
3.3 Problems - difficulties . . . 19

4 Holography **21**

4.1 Introduction - history . . . 21
4.2 Preceding works . . . 21
4.3 Holographic principle . . . 22
4.4 Holographic camera . . . 23
4.5 Optical reconstruction . . . 25

5 Computed Tomography **30**

5.1 Introduction . . . 30
5.2 Segmentation of CT data . . . 32

6 Experiment - probands **34**

6.1 Introduction . . . 34
6.2 Set up experiment . . . 34
6.3 Mobile holographic camera . . . 36
6.4 Protocol low-dose CT . . . 38

7 Methods **40**

7.1 Introduction . . . 40
7.2 Soft tissue measurement . . . 40

7.3 Reproducability of the technique 44
7.4 Results - evaluation 45

8 Problems - considerations 54
8.1 Segmentation of low-dose CT data 54
8.2 Soft tissue shift 55
8.3 Tilted image 59

9 Conclusion 60

Bibliography 62

1 Introduction

Forensic facial reconstruction is a small field within the area of forensic medicine. Forensic odontologists, forensic anthropologists and specific trained artists are performing facial reconstructions. This forensic technique can be useful when other identification methods fail.

Since more than 100 years, scientists are trying to measure the thickness of the facial soft tissue layer, necessary to reconstruct a face. Measurements were performed both on living and dead persons. In the early years, probes and needles were used to measure the soft tissue thickness. Later on, both computers and ultrasonic equipment were introduced. Scientists faced some major problems though: the number of facial measuring points were very limited and the measurements were not accurate. Thus it was not possible to create a soft tissue database. On the other hand, there is a strong need for a reliable database of facial soft tissue thickness in the medical and anthropological forensic world.

The aim of my research project was to develop an easy, efficient and reliable way to measure soft tissue thickness of the face. We used a small number of probands, within the same subcategory (age, ethnic). Holography was the perfect solution to reproduce the facial outline.

In order to develop a new technique to do high precision facial soft tissue measurements, it is necessary to compare the holographic data to bone surface information. Computed Tomography can be a good source to provide these data. It is the first time a technique is developed to do high precision facial soft tissue thickness measurements, resulting in a dense field of measurement points.

2 The human face

2.1 Importance of the face

The human face is an important social tool. We use our face to produce signals expressing emotion and attention. Each face is unique. We are able to notice small variations between faces; this will help us in recognizing and identifying persons. The morphology of the face provides us information about age, health, ethnic group, gender...

The underlying skeleton affects the morphology of the face. The different shapes of the individual skull bones provide a large variation between skulls.
The overlying soft tissue and secondary details such as skin colour, hair, ears, eye colour, wrinkles... will determine the unique character of the face.

2.2 Facial Recognition

A human face reveals lots of information to a perceiver; it can tell about mood and intuition, but it can also serve as an identification tool. Facial recognition is one of the most studied areas in psychology. Still, the process of recognizing and other aspects of face processing were described by Bruce et al [RE1]. They presented a theoretical framework for face recognition. They argued that there are at least seven distinct types of information that can be derived from faces. In facial recognition, two codes are involved in face processing: the pictorial code and the structural code.

A pictorial code is a description of a picture. It is a more abstract level, and it can be used to make yes/no recognition memory decisions. Structural codes give us the ability to distinguish a face from other faces. Codes for familiar faces differ from those formed to unfamiliar faces. The recognition of unfamiliar faces is not simple. And it is well documented that most people find it easier to memorise, interpret and recognise faces of persons belonging to their own racial group ([RE2] Shepherd, 1981; [RE3] Wilkinson). This is called the 'other-race' effect. For example, hair colour can be a distinguishing factor among caucasians, it is not the case in a black or asian population. It is however described that increased contact with a different racial group will improve performance of recognition in that racial group ([RE4] Mc Kelvie, 1978; Shepherd, 1981).

2.3 Facial Structure

2.3.1 Skull

The skull is the term used to name the bonal framework of the head. It is the most complex part of the skeleton as it protects and supports both the brain as well as the organs of sight, smell, taste and hearing.

It is of major importance for physical anthropology . The skull develops under the influences of tension, maturation and growth.

Some knowledge of the correct cranial terminology is important when assessing the skull:

- ***Skull:*** the entire skeletal framework of the head.
- ***Cranium:*** the skull minus the mandible.
- ***Calvarium:*** the cranium minus the face.
- ***Mandible:*** the lower jaw.
- ***Splanchnocranium:*** the facial skeleton.
- ***Neurocranium:*** the brain case.

There are 22 bones in the skull: 6 unpaired and 8 paired; 14 facial bones and 8 cranial bones. Although the hyoid is often grouped with the skull, it is usually not considered a part of it. The bones of the skull unite along serrated joints known as sutures. Most sutures take their names from the two bones of the skull that go together to form the suture. But there are 5 exceptions to this rule:

- coronal suture: between frontal and parietals.
- Sagittal suture: between the two parietals.
- Lambdoidal suture: between parietals and occipital.
- Baselar suture: between sphenoid and occipital.
- Squamosal suture: between parietal and temporal.

Description of the bones of the skull:

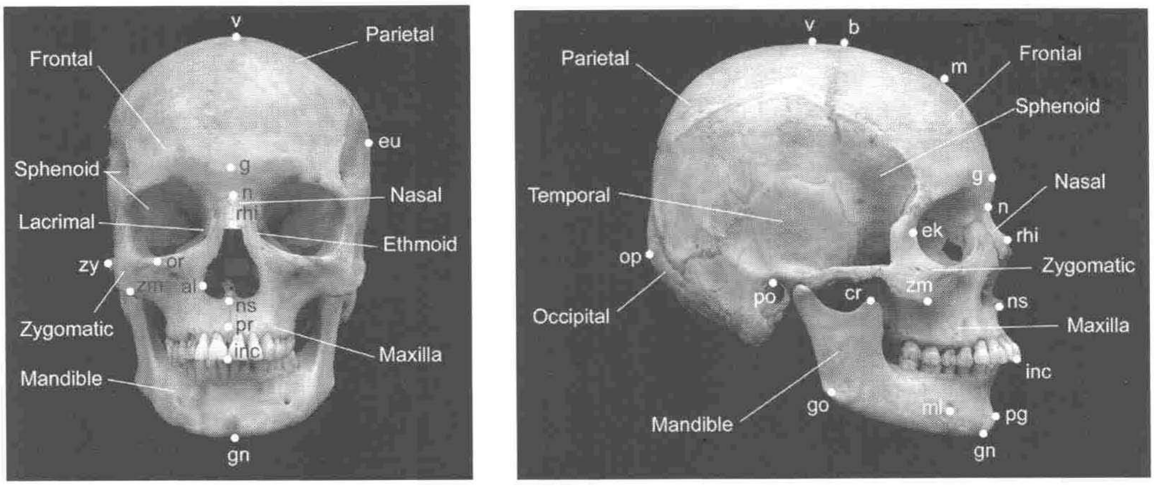

Figure 2.1: Bones of the skull.
Left: frontal view.
Right: lateral view.

Frontal bone: forms the forehead and the upper part of the orbital cavity. Important is the supra-orbital ridge, a prominence above the orbits, often seen in males.

Parietal bones: compose part of the top and the sides of the cranium, posterior of the frontal bone.

Temporal bones: form the lower, lateral sides of the cranium.

Occipital bones: form the back and the base of the cranium. Not so important in facial forensic reconstruction.

Nasal bones: join the maxillae and the frontal bone.

Maxillae: form the upper jaw.

Zygomatic bones: forms the prominence of the cheek, and can be felt under the skin just below and lateral to the eye socket.

Mandible: separate bone, hinged to the cranium at the temporomandibular joint. The mandible has three important parts: the ramus, the condyle and the coronoid process.

Description of the common cranial landmarks:

Alare (al): the most lateral point on the margin of the nasal aperture.

Bregma (b): the cranial point where the coronal and sagittal sutures intersect.

Coronium (cr): point at the top of the mandibular coronoid process.

Ectoconchion (ek): the most lateral point on the orbital margin.

Euryon (eu): the cranial point at the greatest cranial breadth.

Glabella (g): the most prominent point between the supra-orbital ridges in the midsagittal plane.

Gnathion (gn): the most inferior midline point on the mandible.

Gonion (go): point at the centre of the mandibular angle.

Incision (inc): point where the central incisors meet on the incisal line.

lambda (l): intersection of the sagittal and lambdoidal sutures in the midplane.

Mentale (ml): the most inferior point on the margin of the mental foramen.

Metopion (m): cranial midline point on the frontal bone where the elevation of the curve is greatest.

Nasion (n): midpoint of the suture between the frontal and the two nasal bones.

Nasospinale (ns): midline point of a tangent between the most inferior points of the nasal aperture.

Opisthocranion (op): the midline cranial point on the occipital bone, most distant from the glabella.

Orbitale (or): most inferior point on the orbital ridge.

Pogonion (pg): most anterior midline point on the skin.

Porion (po): the uppermost point on the margin of the external auditory meatus.

Prosthion (pr): most anterior midline point on the alveolar process of the maxilla.

Rhinion (rhi): midline point at the inferior end of the internasal suture.

Vertex (v): highest midline cranial point on the zygomaticomaxillary suture.

Zygion (zy): most lateral point on the lateral surface of the zygomatic arch.

Sex determination of the skull:

Due to the influence of interpopulation variation, sex determination from the skull alone may be problematic; there is a certain overlapping of the two sexes. Stewart [SK1] showed he could determine the sex of an entire adult skeleton with 90-95 % accuracy, and 80 % for the skull alone. He also stated that female measurements are 92 % of the male measurements.

Krogman and Iscan [2D2] investigated 750 skeletons and had 100 % success rate when sexing the entire skeleton, 95 % with pelvis alone, and 92 % with skull alone. It should however be pointed out that the male/female ratio of the specimens investigated was about 15/1.

Absolute differences seldom or never exist, and many intermediate skull forms do exist. Krogman and Iscan [2D2], White and Folkens [SK2] and Iscan and Helmer [SK3] did find some distinguishing characteristics. The female skull is generally smaller, smoother and more gracile than the male. The forehead contour in the female is higher, more rounded, more vertical and smoother than in the male.

Supra-orbital ridges are more prominent in males than in females (fig. 1.2). The glabellar region is larger in the male. Female skulls have sharper orbital margins, the orbits are higher and more rounded. Muscle ridges, especially on the occipital bone, are larger in males. Also the mastoid processes are larger in males. The male mandible has a greater body height, is larger and thicker.

Figure 2.2: Sex determination of the skull.
Left: male skull. Right: female skull.

These variations in skulls lead to differences between male and female faces. Enlow [SK6] pointed out that the male face is typically larger, with a larger and more protrusive nose, and more deep-set eyes. Typical is the bulging glabella and the supra-orbital ridges.

<u>Race estimation of the skull:</u>

The skull is the only area from the skeleton from which an accurate race estimation may be obtained. Nevertheless, it is a difficult assessment to determine the racial affiliation; classifying groups on the basis of facial appearance is not evident - Sauer [SK4], Brothwell [SK5].There is some genetic mixing, due to migrating populations around the world. Secondly, there are overlaps between different racial groups, and thirdly there is much variation within the same racial group. The most common racial groups are Caucasoid, Negroid and Mongoloid.

CAUCASOID skull	NEGROID skull	MONGOLOID skull
long, narrow shape	long head shape	round head shape
narrow nasal opening	wide nasal aperture	medium-width nasal aperture
little or no prognathism	strong alveolar prognathism	moderate prognathism
depressed nasal root	low rounded nasal root	short nasal spine
moderate supra-orbital ridge	sharp upper orbital ridge	no brow ridges
narrow interorbital distance	wide interorbital distance	wide facial breadth
depressed glabella	rounded glabella	prominent zygomatic bones
large mastoid processes	bregmatic depression	flatter face

2.3.2 Soft Tissue

The skull is covered by a soft tissue layer, consisting of fat, muscles, vessels, salivary glands, nerves and skin (fig. 2.4). The facial outline is mostly determined by the musculature and fat. Because muscles control expressions of the face, they are sometimes referred to as muscles of "facial expression". They also act as sphincters and dilators of the orofices of the face (i.e. orbits, nose and mouth).

Facial muscles can be divided in 4 groups:

- orbital group
- nasal group
- oral group
- other

Gerasimov (1971) [FR12] stated that when reconstructing a face, the artist / scientist should have a deep understanding of the muscles of the face and neck, their attachments, origins and actions. Research into facial soft tissue through dissection will allow an anatomically correct facial outline (fig. 2.5).

Figure 2.3: Race stereotypes of the skull.
a) caucasoid skull. b) negroid skull. c) mongoloid skull.

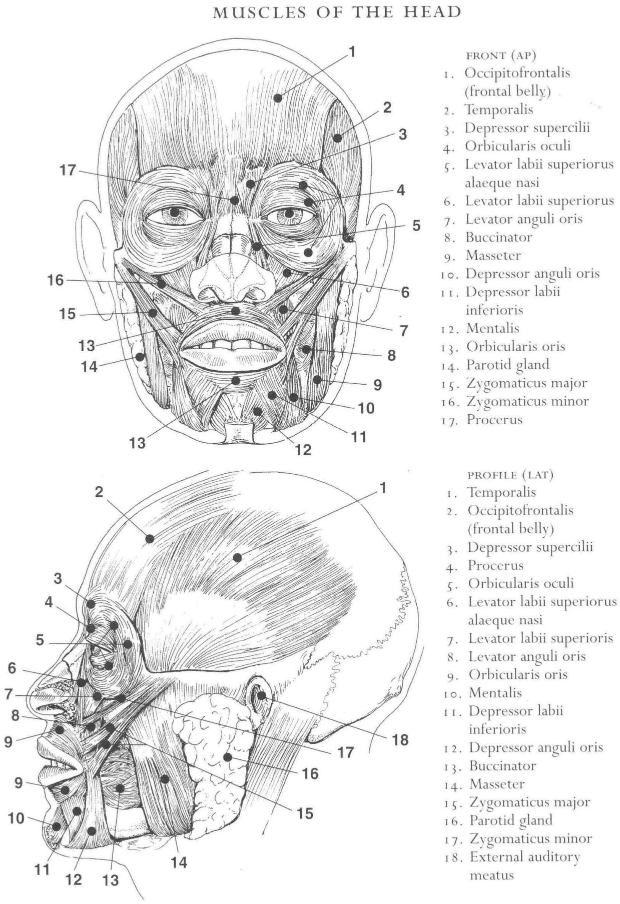

Figure 2.4: Muscles of the head. Image source: Richard Neave.

Figure 2.5: Facial muscles and markers, showing main tissue depth at specific anatomical points, in an intermediate stage of a plastic reconstruction, according to the Manchester method. Image source: Richard Neave.

3 Facial Reconstruction

3.1 History - overview

Facial reconstruction, the scientific art of visualising faces on skulls for the purpose of identification, has been exercised for over a century. Scientific art is the use of artistic skills following scientific rules.

Within forensic anthropology, facial reconstruction is used when all other alternatives are unsuccessful. The technique is indicated when dealing with burnt, severely mutilated, skeletonised or decomposed bodies or remains. The aim is to get a resembling image of the person prior to death. The reconstruction may be presented on television or in newspapers. Hopefully someone, somewhere will be able to identify the deceased.

Anatomists in the late 19th century conducted much of the early research in facial reconstruction. There have been many applications of facial reconstruction in the past, including its use in the reproduction of busts from skulls of famous people. Faces of these historical people were created by comparing them with death masks and portraits in order to corroborate the authenticity of skulls found in tombs.

Between 1867 and 1883, the German anatomist Welcker [HI1, HI2, HI3] used two-dimensional reconstructions to discuss the skulls and death masks of Dante, Schiller and Kant. He utilised tissue depths he had collected from cadavers. A variation of this method was used by His [HI4] in 1895, to reconstruct Johann Sebastian Bach's face and compare it to the portraits of the composer that were available. In that period, faces were categorised according to the tissue thickness; average male, average female, and maximum-minimum variations for both sexes. In 1898, Kollman and Büchly [HI5] made a modelled reconstruction of a prehistoric skull, using tissue depth markers and clay. They also compared their results with those of His, and combined the data to obtain mean values, and maximum-minimum variations.

It is generally recognised that there are three different techniques for facial reconstruction:

1. two-dimensional facial reconstruction (2D)

2. video superimposition

3. three-dimensional facial reconstruction (3D)

1. 2D-facial reconstruction

In the 2D-facial reconstruction, an artistic drawing is placed over the representation of the skull. This reconstruction method creates a face from the skull with the aid of soft tissue depth estimates. In 1977, Cherry and Angel [2D1] produced a drawing of the face by using a skull photograph. Krogman and Iscan [2D2] used lateral and frontal radiographs to make tracings (1986). Also George [2D3] used lateral radiographs; he mentioned this data set could be important for calculating facial profiles (1987). Ubelaker [2D4] developed a technique, using soft tissue thickness markers on the skull. A photograph is then taken in the Frankfurt plane. Later, computer-assisted approaches to facial reconstruction became more popular. In 1992, Ubelaker and O'Donnell [2D5] described the F.A.C.E.™ system, which is a a two-dimensional computerised and digitised version of Ubelaker's earlier work. The C.A.R.E.S.™ system also produces composite images, as the result of an overlay of both a photograph and a sketched image, using contours of the skull. The advantage of these computerised systems is that they can produce different composite images from the same skull contour, by using different facial features.

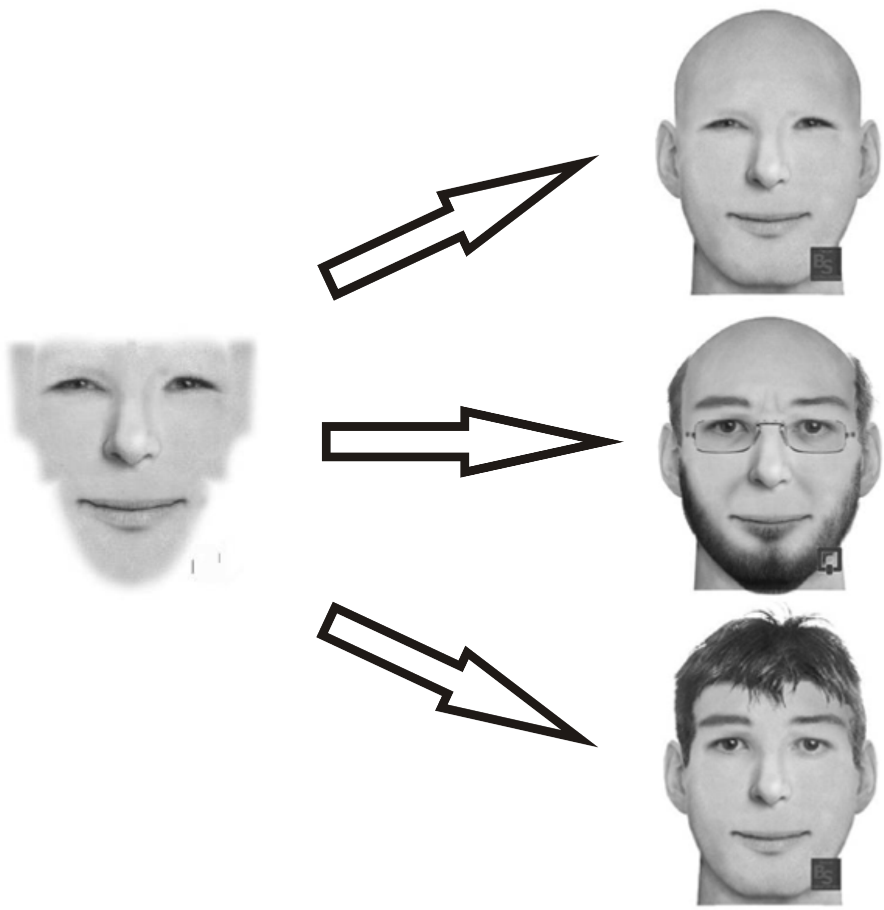

Figure 3.1: Different features of one basic composite picture.

2. video superimposition

The technique of **video superimposition** is used to compare the skull with a pre-mortem photograph; it is an attempt to supply a face for a found skull. The purpose is to establish a close enough relationship between the two images, to state that these belong to the same individual, with a high degree of confidence.

The first image is that of the unidentified skull. The image of the face can be derived from a photograph (most common), or from radiographs.

One of the difficulties of superimposition is the orientation of the skull to the image of the face. Iten [FR1] related the eye level to the external auditory meatus, in order to determine the anterior-posterior tilt. Seta and Yoshino [FR2] mounted the skulls and adjusted the orientation using a joystick. Smeets and Prieels used a combination of relation between the eye level *l* external auditory meatus (fig. 2.3). A robot can digitally move over 6 different axes, in order to get the exact position of the skull. Two video cameras are mounted and fixed; one camera is recording the photograph, the other one is recording the skull. All movements should be recorded digitally, to make the investigation work reproducible (fig. 2.2).

If we want to match the skull and face image correctly, both should have the same size. Maat [FR4] searched on the positioning and magnification of skulls and faces.

The validity of superimposition techniques has always been a point of discussion. Cocks [FR5] compared triangulated anthropological points marked on the skull and on the face photograph, to quantify the comparison. Brown [FR6] argued that it is difficult to find the points on a face photograph.

In a study on 52 European skulls, Helmer [FR7] concluded that skulls were comparable in their individuality to fingerprints. In his work, Helmer defined 34 distinctive points on the skull, which very often serve as the reference (Helmer points) [SK3].

De Vore [FR8] pointed out that photographic superimposition is of better use in exclusion rather than inclusion. Brown [FR9] reported that Australian courts accept video superimposition as an identification method.

Figure 3.2: Skull mounted on robot.
Video superimposition technique used by Smeets and Prieels.
Image source: Bregt Smeets (on unpublished work)

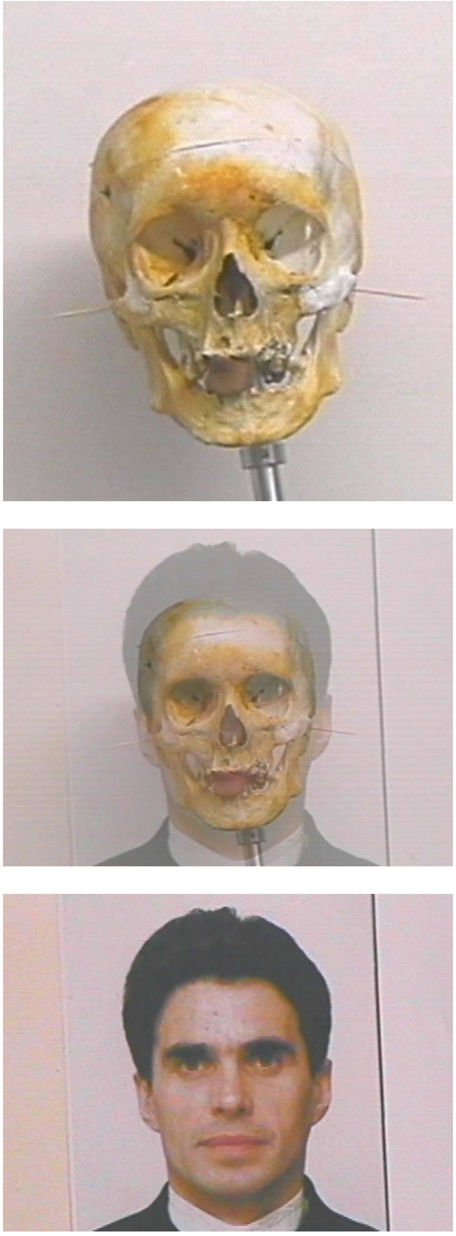

Figure 3.3: Superimposition of a picture over an unknown skull.

3. 3D-facial reconstruction

Several methods exist which utilise soft tissue depth markers fixed to the skull or a cast. The soft tissue of the face are then built up with clay, plasticine or wax. The method is dependent on the knowledge of certain features of the skull, as well as the use of tables of mean values of facial soft tissue thickness, measured at some specific landmarks. Neave [FR10] said that it is often a collaboration between the anthropologist and the artist, where the artist works using instructions from the anthropologist.

Normally the reconstruction is made on a copy of the skull, to avoid any damage to the skull; it can be a plaster model or a rapid prototyping model. In case of a plaster model, an alginate impression is taken of the skull. Both skull and mandible are fixated in a central relation (rest position of the two jaws without occlusion). They can be fixed using dental wax.

The choice of tissue depth data is determined by sex, age and ethnic origin of the skull. Holes are drilled into the model , rectangular to the model surface. Markers (rubber or wooden pegs) are cut off to the length according to the soft tissue thickness at that specific landmark, and fixed to the model.

The Russian anthropologist Gerasimow was a pioneer in developing the Russian or anatomical method of three-dimensional reconstruction. The face was rebuilt muscle by muscle, without the use of tissue depth measurements. He believed there was a correlation between details of nose, eyes, mouth, ears, and the relief of the skull at specific areas [FR12].
The following subcategories of 3D facial reconstruction exist:

3-1: strip plastic facial reconstruction.

In this technique, strips of clay are used to fill up the spaces between the landmarks. The skin is formed by filling in any gaps and smoothing the whole surface [FR11]. The disadvantage of this method is that the surface information between landmarks remains inaccurate. In areas with few landmarks, this may have an influence on the changes in contour over the soft tissue surface. Any interferences noticed from the skull, should be added to the reconstruction in a second step.

3-2: anatomical facial reconstruction

As in the former technique, markers are placed to the landmark sites corresponding to tissue depth values, found in reference tables. The Manchester method of facial reconstruction is developed by Neave and Wilkinson [FR10].

Plastic eyeballs are positioned in the orbita. One by one, the muscles of the face are modelled on the skull. Position and form of these muscles are related to the shape and form of the face. The tissue depth pegs can act as a guide, but sometimes these pegs are misleading, according to the specific morphology of the skull. The reconstruction practitioner should keep in mind that the soft tissue thickness data are average tissue measurements that will not be accurate for an individual skull.

In the next stage, a layer of clay will reconstruct the subcutaneous fat and skin. Every detail of the reconstructed face must be based on scientific assessment of the skull morphology. Hairstyles, wrinkles, beard, scars and glasses should only be added if these are suggested according to the post-mortem information provided by the forensic pathologist. False information may mislead the observer. In contrast, Taylor [FR13] uses eye colour, skin tone etc from population statistics. In the Manchester method, practitioners prefer to add only those facial features that are certain.

Figure 3.4: Different steps in anatomical facial reconstruction.
Skull, muscles, fat, skin. Image source: Richard Neave.

3.2 Soft tissue measurement

Collecting data on facial soft tissue measurements is important in order to perform an adequate reconstruction of the face. The first research into facial soft tissue depth was done by the early practitioners of facial reconstruction. They provided their own tissue depth measurements. Welcker [HI3] carried out the first documented research in 1883. He collected measurements from cadavers by sliding the

blade of a scalpel through the tissue at predefined landmarks. The blade was then marked and the depth of the scalpel's penetration was measured. He studied 13 white male cadavers of middle age. In 1895 His [HI4] used a modification of Welcker's technique to obtain tissue depth information; he used a needle pushed into the skin of the cadaver, which displaced a rubber disc, representing the depth.
Kollman and Büchly (1898 [HI5]) expanded on His's research; they bused a needle, covered on soot, with the clean area of the needle indicating the thickness of the soft tissue.
Other earlier research on soft tissue thickness was done by Czekanowski (1907 - [STM1]), Berger (1965 - [STM2]), Leopold (1968 - [STM3]), Suzuki (1948 - [STM4]).
In 1980, Rhine and Campbell [STM5] took measurements from Black American cadavers, they chose unembalmed bodies (deceased no longer than 12 hours) to minimise post-mortem effect on the soft tissue. Rhine and Moore (1982 - [STM6]) did a similar work, measuring tissue depths on White Americans.

There are some problems with cadaver studies (ctr later); different and more accurate of soft tissue thickness measurements were therefore studied.

One of the new techniques was to take different measurements from cranial radiographs. Research on making soft tissue measurements on White Europeans was done by Bankowski (1958 - [STM7]) and Leopold (1968 - [STM3]); Weining (1958 - [STM8]) and George (1987 - [2D3]) investigated craniographs of White Americans.
A study of Aulsebroock (1996 - [STM9]) measured the faces of 55 male Zulus, using both radiographs and ultrasound. Phillips and Smuts (1996 - [STM10]) studied 32 Mixed Race subjects using CT scans, whilst Sahni (2003, [STM11]) took MRI scans of a population of 60 Indians.
Ultrasound was introduced as a safe and effective way to measure soft tissue thickness. Helmer (1984, [STM12]) studied 123 White European subjects. The results were divided into ten-year interval age groups and by sex.
Lebedinskaya and her team (1993 - [STM13]) studied 1695 individuals, from nine ethnic groups within the former USSR.
De Greef (2005 - [STM14]) used an ultrasound-based system to measure soft tissue thickness of 967 Caucasians.

3.3 Problems - difficulties

Not only the problem of accuracy of soft tissue depth data, but also the lack of understanding of how soft tissue changes between the landmarks, make facial reconstruction widely criticised. Many studies showed that the lack of accurate and comprehensive soft tissue depth data is one of the factors contributing to the inaccuracy of facial reconstruction [FR14, FR15]. The problems regarding the soft tissue depth data are both the mode of collection of the data, and the choice of landmarks. The results of the cadaver measurements are not considered to be an accurate representation of the amount of tissue on the face in a living person (shrinkage, loss of muscle tone, general signs of putrefaction). One problem associated with the ultrasonic technique is the placing of the pen tip at the correct anatomical point over the skull; it is not always simple to locate these points. Values of measurements also depend on the angle of the needle or the ultrasound probe. A slight angle deviation can change the measuring results dramatically. An additional problem is the lack of landmarks in some areas (e.g. cheek area); this makes it difficult to find the right cheek contour [FR16].

These measurement datasets have further limitations; there is only a small number of subjects in the soft tissue depth studies, and there are limited data available of different age, sex and race groups.

In preparation of the 2nd International Conference on Reconstruction of Soft Facial Parts in Remagen, Germany (2005), participants were asked to perform a reconstruction on an unidentified skull (fig. 3.5). A Rapid Prototyping (RP) model of the skull - prepared by the CAESAR RP group - and a report of the anthropological examination - done by the Institute of Anthropology of the University of Goettingen - were presented to the participants (fig. 3.6). They had the choice between a drawing, 2D- and 3D-computer reconstruction and a sculpture.

The results were rather fascinating as they showed a large variation on reconstructions. The whole experiment showed that both science and artistic skills will influence the result of a facial reconstruction.

2nd International Conference on Reconstruction of Soft Facial Parts (Jens Bongartz, Remagen 2005).

Figure 3.5: Left: unidentified skull.
Right: CT image unidentified skull.
Image source: Jens Bongartz.

Figure 3.6: Rapid Prototyping Replicas of the skull.
Image source: Jens Bongartz.

4 Holography

4.1 Introduction - history

Both in maxillofacial reconstructive surgery [Ho-In1] as in forensic soft tissue measurements, there is a strong need for a contact-free, optical measurement system. This requires a system with a good optical resolution and a short measuring time. Chen [Ho-In2] made an overview of a three dimensional shape measurement using optical methods. Bongartz [Ho-In3, Ho-In4] focused on this issue and stated that none of these techniques were useful for facial measurement; both exposure time and resolution did not meet the medical requirements.

To fulfill the requirements for facial measurements of living persons, the *Holography and Laser technology group* at CAESAR (Center of Advanced European Studies and Research) in Bonn developed a topometry system based on pulsed holography.

Gabor [Ho-In5] invented the concept of holography in 1947, for which he was rewarded the Nobel Prize in 1971. In his historical demonstration of holographic imaging, a collimated beam of monochromatic light was used to illuminate a transparency consisting of opaque lines on a clear background. The interference pattern produced by the directly transmitted beam and the light scattered by the lines on the transparency were recorded on a photographic plate. Gabor wanted to use a lensless imaging system, as he found that the quality of the electron lenses was too poor. He recorded an electron wave field on a medium, and reconstructed it optically at a later time. He named the interference pattern optical holography, from the Greek *holos* (whole) and *graphe* (writing). Although this application of holography was never used in electron microscopy, the development of the laser led to optical holographic surfaces.

4.2 Preceding works

In the Holography and Laser Technology Group (Prof. Hering) at the CAESAR foundation in Bonn, the use of analog portrait holography was introduced as a tool for facial topometry, using a short-pulsed green laser.

The development and improvements of this approach were described in five PhD theses and in many articles.

The first thesis on holographic facial measurement was written by Bongartz [Ho-In4]; he described the advantages of the fast capture as an optimal tool for the measurement of faces of living persons. He used a diffuser screen and a CCD camera to create the real image digitization. His work included the whole holographic recording process, several medical considerations, as well as the scattering properties of the skin.

Giel [Ho-In6] used inverse filtering and iterative deconvolution in conjunction with holographic real images. He introduced a laser speckle projection to improve the skin contrast, and discussed the influence of moving apertures and additional aperture by adding mirrors.

Frey [Ho-In7] used a CMOS flatbed scanner instead of a diffuser screen and a CCD camera, to digitize the real image directly. The quality of the real image improved so much, that no further structured illumination was needed. From now, eye-safe recordings were possible.

Thelen [Ho-In8] concentrated on contrast based methods for extracting three-dimensional information from two-dimensional projections (surface extraction). She evaluated twelve different mathematical operators for contrast measurement; the XSML (Extended Sum Modifies Laplacian) performed best.

Hirsch [Ho-In9] presented a full-sized area detector to replace the platbed scanner. Thus he eliminated the shortcomings of speed, dynamic range, mechanical instability and image artefacts. This scanner uses a X-ray flat-panel detector (FPD) as an area sensor to capture each image at once. Hirsch also introduced the digital holographic topometry, where a CCD sensor is used to digitize the real image.

4.3 Holographic principle

In conventional imaging techniques, a picture of a three-dimensional object is projected on a light-sensitive surface by a lens. Only the amplitude is registered, all information on the relative phases of the light waves are lost.

Holography is unique because of the recording of the complete wave fields; both phase and amplitude are recorded at the same time, without using lenses. The holographic information is generated by superposition of two coherent beams, a reference wave and a wave scattered from the object. The photographic plate contains the hologram, which shows no resemblance to the original object, as it is inscribed in a coded form. By illuminating the hologram with a respective beam, the real image can be reconstructed. To the observer, the reconstructed wave is indistinguishable from the original object [Ho-Pr1], yet usually monochromatic.

The use of the laser system is very important in the holographic recording of human faces. The recording of living persons requires a short pulse duration and a long coherence length of the light beam. Additionally, the pulse energy has to be adapted to the sensitivity of the recording subject, and it has to be high enough to expose the photographic emulsion on the holographic plate in a homogeneous way.

4.4 Holographic camera

Evaluation and validation of the recording procedure was done with a Geola GP-2J holographic camera. The camera uses a frequency doubled Nd:YLF laser in an oscillator-amplifier arrangement; it is especially designed for portrait holography. The maximum pulse energy is 2J at 526.5 nm with a pulse duration of 35 ns. The laser output is split into three beams. The two illumination beams serve for homogeneous illumination of the subject. They are expanded by concave lenses and led through diffuser plates, which make the holographic recording eyes-safe. The reference beam leaves the camera through a pinhole and a concave lens at the output ports of the laser. The expanding spherical wave is led by mirrors to the holographic plate. The test person is sitting in front of the holographic camera, at a distance of approximately 60 cm to the holographic plate.

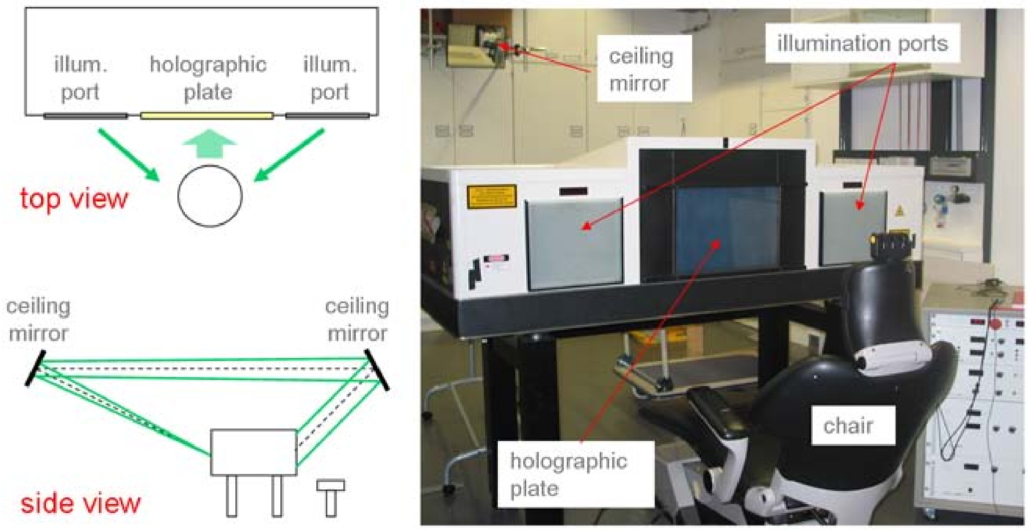

Figure 4.1: The laboratory holographic camera.
Schematic top view, side view and photograph of the configuration.

The reference beam is superimposed to the fraction of the scattered light from the face that reaches the photosensitive holographic plate. The exact distance of the person in front of the camera is not critical. An adjustment on image sharpness is not necessary as there are no lenses between the face of the person and the holographic plate. After triggering the laser pulse, the three-dimensional information is stored in the holographic plate [Ho-In4, Ho-In6, Ho-In7]. The hologram is ready for chemical processing, and the recorded person can leave.

Figure 4.2: The double sided diffuser at one of the illumination ports of the mobile camera.

There is a slight shift in wavelength compared to the continuous wave Nd:YAG reconstruction laser with a wavelength of 532 nm. This shift may be corrected numerically by inducing a scaling into the reconstructed real image.

The processing of the hologram plate is usually performed manually. The cassette with the exposed plate is chemically processed in a dark room. The holographic recording material is a high-sensitive photographic film (silver-halide salt crystals) embedded in gelatine coated on a glass plate. It has a resolution of about 3000 lines/mm, which is far above the minimum of 2300 lines/mm necessary for portrait hologram recordings [Ho-In4].

Phase or amplitude holograms can be generated, depending on the chemical processing. Amplitude holograms have a lower diffraction efficiency, since the modulation is realised through absorption in the dark regions. On the other hand, phase holograms are more efficient in respect to the diffraction of light as they work with a phase modulation. There is also some additional noise due to the bleaching procedure. In the course of this thesis only phase holograms were used. Bjecklhagen [Ch-Pr1] described the optimal chemical processing for pulsed holograms.

As an alternative, an X-ray film developer and an adaptation of the chemistry can be used to provide an automated chemical development. Since automated processing is only possible for flexible films, it needs to be fixed on a glass plate. Due to problems in fixing the film to a plate, plates for holographic recordings are preferred [Ch-Pr2, Ch-Pr3].

4.5 Optical reconstruction

Reconstruction beam

The coded three-dimensional information stored in the hologram can be decoded through illumination with the complex conjugate reference beam. The complex conjugate reference beam is chosen to create the real image, since the virtual image cannot be used for topometry purposes. The reconstruction is done on relatively small optical table (1.70 m x 1.20 m), so the beam had to be folded several times.

The light source is a diode pumped frequency-doubled Nd:YAG laser with continuous wave single longitudinal mode operation at a wavelength of 532 nm. Behind the laser, the beam is enlarged by a 1:10 telescope, followed by an adjustable attenuation and a convex lens, which is responsible for the primary formation of the beam. A periscope lifts the beam to the appropriate height on the optical table. The beam then passes the first reflection mirror which is mounted on a rail. After a second deflection the beam impinges on the spherical mirror, where the divergent beam is reflected to form the conjugate reference beam, which is convergent. The plate holder can be adjusted in orientation and position towards the reconstruction beam. The distance between the spherical mirror and the hologram plate is fixed. A flat panel detector is mounted on a translation stage and is positioned at the site of the real image.

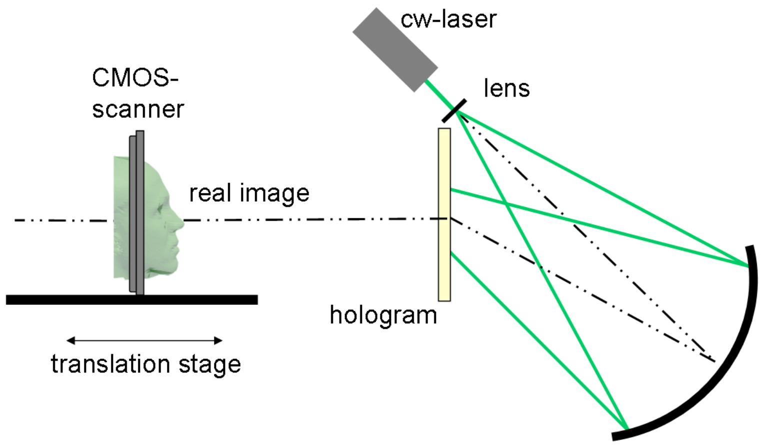

Figure 4.3: Optical reconstruction with the complex conjugate reference beam.
The real image appears as a three-dimensional light field at the former position of the recorded object.

The orientation of the hologram plate towards the reference beam during recording is crucial. During the optical reconstruction, the final alignment of the hologram plate towards the reconstruction beam is done under direct visual control. The absence of any aberrations is the criterion for a good reconstruction quality. The exact parallel orientation between the holographic plate and the flat panel detector is essential in order to avoid a 'tilted image' [OR1].

Scaling due to wavelength shift

A major source of scaling is the relation u of the wavelength between the reconstruction beam and the

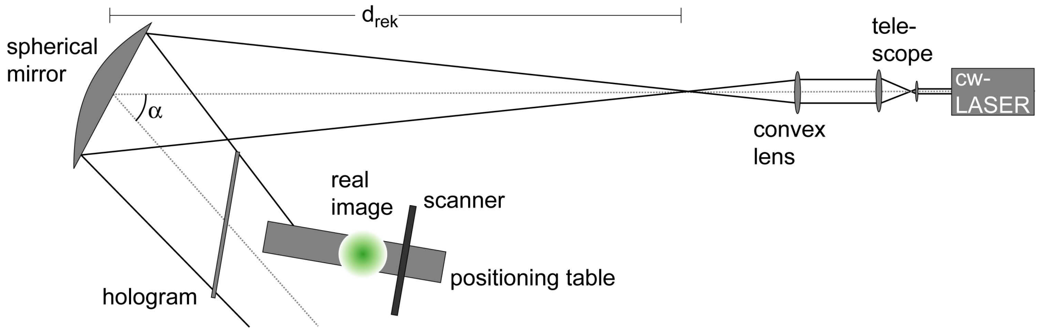

Figure 4.4: The conjugation of the beam is realized with a spherical mirror. The tilt of the mirror α introduces a cylindrical aberration to the reflected beam.

reference beam. For the mobile holographic system, both lasers have the same wavelength of 532 nm, u = 1. The lab holographic system operates with an amplified Nd:YLF laser at 526,5 nm wavelength, u = 1.0104. This numerical scaling correction can be done easily [Ho-In4].

Digitizing of the real image

The real image, generated through the optical holographic reconstruction is an exact copy of the person's face. The digitising of the real image is realised through the recording of a set of two-dimensional projections at different axial positions of the three-dimensional real image. Bongartz named the whole procedure hologram tomography [Ho-In4].

Figure 4.7 shows a set of tomograms through the real image at progressing positions. Several regions of the face are imaged sharply while the other regions of the face are unfocused. The focus progresses from the tip of the nose up to the ears.

Hirsch [Ho-In9] implemented a flat panel area detector, which captures each slide at once.

The traditional CMOS scanner showed some typical shortcomings in terms of speed, dynamic range, artefacts and stability. The scanning of one slice needs between 25 s and 60 s, depending on the scan resolution of 150 dpi-600 dpi. The time for digitising 256 slices of the real image is between 1.5 h and 3 h. By manually tuning the orientation of the hologram plate, an optimal placement can be achieved. The image quality of a CMOS scanner is poor, it is impossible to cover the dynamic range of a hologram.

Hirsch [Ho-In9] described a further improvement of the digitization of the real image.

An area sensor was custom designed, capable of capturing each slide at once. The sensor used is a flat panel detector based on the PaxScan 2520 V by *Varian*. The resolution of this X-ray sensor is 200 dpi. The effective size of the active area is roughly 25 cm x 20 cm, the total number of pixels is 1920 x 1536. This new sensor generation for high performance digitization brought many advantages to the traditional hologram topometry method. The speed was improved by a factor 300, the time needed for a real image scan was reduced to 30s. The mechanical stability was improved and the device had

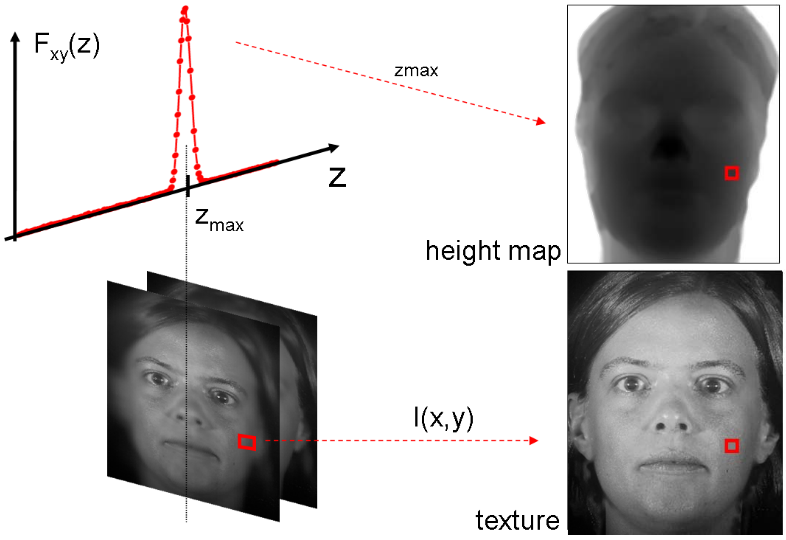

Figure 4.5: For each lateral point (x, y), the focus values $F_{xy}(z)$ are maximized, which delivers the desired z-coordinate. Simultaneously, the height information of the face and the corresponding texture are extracted.

a higher dynamic range.

Figure 4.6: The VRML-model combines the surface data *left* with the precisely fitting texture file *middle* to form the final digital model *right*.

As the new detector is very light-sensitive, the hologram quality is less critical than it was before. Even holograms with a very low image contrast may still be used for the reconstruction.

Surface extraction

Next step is to find the object surface. After digitization of the real image, the object is represented as focussed points in the image volume. Such, the digitized volume is an overlay of focussed and unfocussed points. Focussed regions carry more information in a higher spectral range than unfocussed regions. A measure for the degree of focus is given by a mathematical operator measuring image contrast, as the local contrast in small neighbourhood will be larger for focussed points.

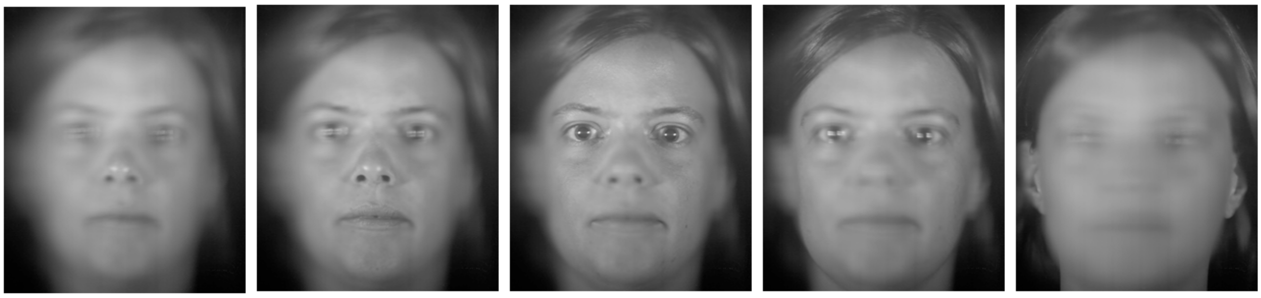

Figure 4.7: Example for set of tomograms of the real image at different positions. In each slice, some of the areas of the face are sharp, while others are unfocussed. The focus progresses from the tip of the nose up to the ears.

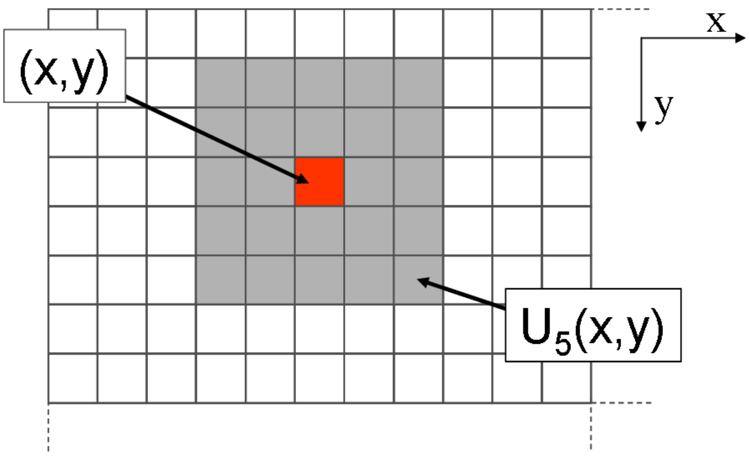

Figure 4.8: Sketch of a local pixel neighbourhood $U_5(x, y)$ of the point (x, y) with the size of 5x5 pixels.

Finding the maximal focus values is necessary in order to extract the surface information of the recorded object or face. Comparing focus values along the z-axis delivers a z-value for each lateral point.

The extracted surface can be visualised through the height map, which displays the z-values as coded gray values; low numbers are dark colours (front) and high numbers are light (back). The height map is a parallel projected surface and gives the position of the highest sharpness in the real image. The height map is used to extract the brightness information from the image volume. This extracted image is called the texture image. This grey scale picture can be dyed with one colour, to create a more realistic appearance. The height map and the texture image are combined into the final digital computer model.

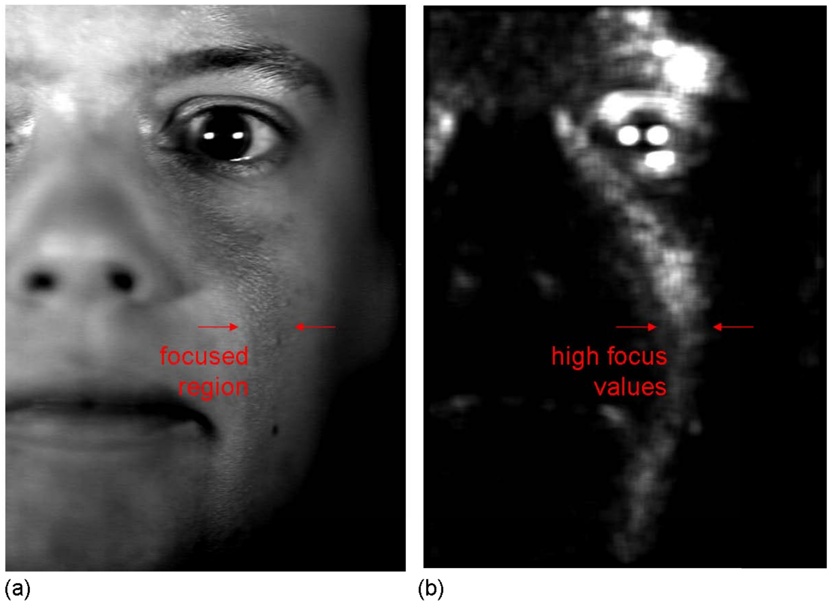

Figure 4.9: a) one slice of a typical scan shows clear focus profile, which is clearly extracted by b) the focus value. White corresponds to high contrast values, black to low contrast values.

Surface visualization

The Virtual Reality Modelling Language (VRML) is used to store the 3D-model as a plane text file. The graphical file format is intended to be a universal exchange format for multimedia and is used in a variety of applications such as engineering and scientific visualization [OR2]. It can be displayed using a VRML-plugin, for example the *blaxxun contact* plugin (*http://www.blaxxun.com*). It additionally provides information about illumination, background color and the viewing position.

The actual topometry information is given as a set of three-dimensional points (x,y,z), where the neighbouring points are connected to form a trigonal model. The texture image is mapped precisely on the object surface.

In order to add the texture to the polygonal model, the node positions are projected into the texture image coordinate system. These projected node coordinates are also written in the VRML-file, so that the texture is positioned correctly in the resulting model.

5 Computed Tomography

5.1 Introduction

In order to develop a new technique to do high precision facial soft tissue thickness measurements, it is necessary to compare the holographic data to bone surface information. Computed Tomography (CT) can be a good way to provide these data.

We have been familiar with radiographs for about a century now. Anatomy is presented on the analog film as a continuum with nearly arbitrary fine transitions. The human eye does not recognise any steps in intensity; only arbitrarily fine gradations of grey levels and continuous transitions for contours are given.

Computed Tomography was the first widely used radiological imaging modality which exclusively provided computed digital images instead of the well known directly acquired analog images. It also offered images of single discrete slices instead of a super-positioned images of complete body sections.

For an understanding of Computed Tomography it may be helpful to view the human body as a finite number of discrete slices and volume elements. Each single scan aims to determine the composition of one transverse cross-section. The slice or section can be imagined as composed of discrete cubic volume elements. The value of each volume element is displayed in one picture element of the digital image matrix. For volume elements we often use the term *'voxel'*, and for picture elements the term *'pixel'*. In principle, a slice image can be generated in arbitrary orientation. For CT, mostly a transverse plane (x/y-plane) is scanned directly. The z-axis, orientated perpendicular to the scan and image plane, is thereby aligned along the axis of rotation of the scanning system, parallel to the body's longitudinal axis. Sagittal body sections are approximated by y/z-planes, coronal sections by x/z-planes. A conventional radiograph shows a modulated distribution of radiation intensity and always offers a superposition image. Each picture element displays the sum of all contributions to attenuation [CT1].

Image contrast is defined by the difference in intensity of two neighbouring picture elements or regions. Contrast in radiographs is dominated by structures with high attenuation such as bone and contrast media, or by differences in object thickness. Soft tissue structures provide low attenuation; even the introduction of improved detector systems or digital data processing will not alter the situation. For slice images, contrast is given directly by the attenuation values of neighbouring volume elements. Contrast is determined by the composition of the tissues, while neighbouring or superimposed structures have no or only very little influence [CT1, CT2, CT3, CT4].

For survey radiographs, the relative distribution of the X-ray intensity is recorded; for classical radiographs only the grey value pattern is utilised to derive a diagnosis. In CT, in addition to the intensity I attenuated by the object, the primary intensity I_0 has to be measured in CT to calculate the attenuation value along each ray from the source to detector.

CT measures and computes the spatial distribution of the linear attenuation coefficient u. However, the physical quantity u is not very descriptive and is strongly dependent on the spectral energy used. The attenuation coefficient is displayed as a so-called CT value relative to the attenuation of water. In honour of the inventor of CT, CT values are specified in Hounsfield Units (HU). For a tissue with attenuation coefficient u_T the CT value is defined as

$$\text{CT value} = \frac{(u_T - u_{water})}{u_{water}} \cdot 1000 \text{ HU} . \tag{5.1}$$

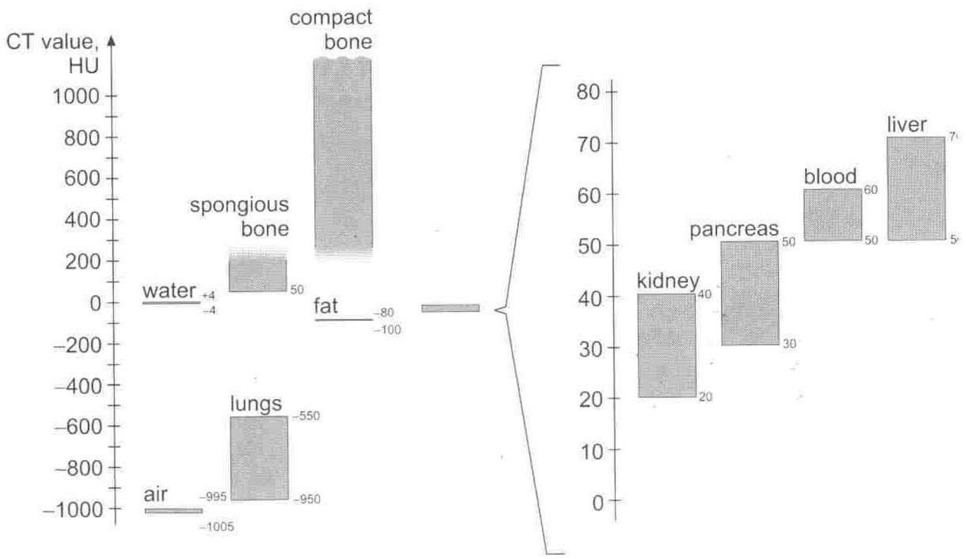

Figure 5.1: The Hounsfield scale. CT values characterize the linear attenuation coefficient of the tissue in each volume element relative to the μ-value of water. The CT values of different tissues are therefore defined to be relatively stable and to a high degree independent of the X-ray spectrum.

On this scale, water and each water-equivalent tissue with $u_T = u_{water}$ has the value 0 HU by definition. Air corresponds to a CT value of −1000 HU. Lung tissue and and fat exhibit negative CT values due to their lower density and the resulting lower attenuation ($u_{lung} < u_{water}$). Most other body areas exhibit positive CT values , due to the physical density of muscle and most of the soft tissue. For bone, the increased density is responsible for a higher attenuation and therefore for higher CT values, up to 2000 HU. CT values of bone are more strongly dependent on X-ray energy than water, and increase with reduced high voltage settings, as known in the contrast settings in conventional radiographs. The Hounsfield scale has no upper limit. For medical scanners a range from -1024 HU up to $+3071$ HU is provided. Consequently, 4096 ($= 2^{12}$) different values are available (= 4096 grey levels) [CT1].

Spiral CT means the fast and continuous scanning of complete volumes; it replaces the sequential scanning of single slices, which means only discrete sampling along the z-axis. The patient is transported continuously through the tube at a speed of one to two slice collimations per 360° rotation. For multi-slice systems and sub-second rotation times, the table speed can be increased [CT5]. The image reconstruction in spiral CT is in principle the same as in sequential CT; identical algorithms, convolution kernels and same hardware are used. However, an additional pre-processing step is required, the so-called *z-interpolation*. The calculation of images from any 360° spiral data segment leads to artefacts, since different object sections are measured at start and at the end of any such segment. The resulting artefacts correspond exactly to the motion artefacts known from sequential CT.

5.2 Segmentation of CT data

In many medical-imaging applications, image segmentation plays a crucial role, by automating or facilitating the delineation of anatomical structures and other regions of interest. The growing size and number of these medical images have necessitated the use of computers to facilitate processing and analysis. Image segmentation algorithms play a vital role in numerous medical-imaging applications.

Partial-volume effects are artefacts that occur where multiple tissue types contribute to a single pixel, resulting in a blurring of intensity across the boundaries. The most common approach to face partial-volume effects is to produce segmentations that allow regions to overlap, called soft segmentations. Standard approaches use hard segmentations, a binary decision on whether a pixel is inside or outside the object.

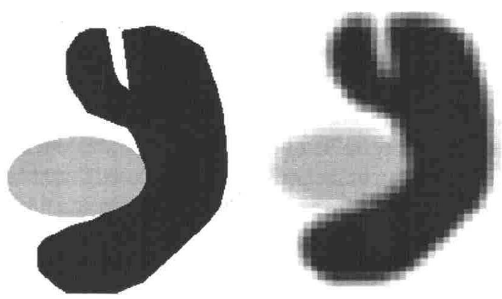

Figure 5.2: Illustration of partial-volume effects.
Left: ideal image.
Right: acquired image.

Thresholding is a simple and effective way for obtaining a segmentation of images in which different structures have contrasting intensities. Thresholding does create a binary partitioning of the image intensities. The segmentation is achieved by grouping all pixels with intensities greater than the threshold into one class, and all other pixels into another class.

6 Experiment - probands

6.1 Introduction

Traditional methods for static object topometry show good results when using a long acquisition time. Topometry of living persons is much more complex, and when using the traditional methods, artefacts may occur.

To overcome these shortcomings, holographic topometry was developed to digitize human faces. Living individuals can be captured without moving artefacts due to the extreme short acquisition time. Additionally, the pulse energy has to be high enough to illuminate the whole face in a homogeneous way.

Many aspects of the holographic topometry have been described in previous dissertations. Bongartz [Ho-In4] described the method for the first time. He implemented speckle illumination and the use of a mirror setup [Ho-In6]. Frey introduced a direct real image scanning [Ho-In7], and Thelen focussed on the reconstruction methods and image refinement [Ho-In8]. Finally, Hirsch introduced the digital holographic topometry by introducing a CCD sensor to record the hologram [Ho-In9].

In the setup for this experiment, we used the first mobile camera for daylight capture. The persons are captured into a pulsed portrait hologram. The camera is described in chapter 6.3.

After capture, the hologram plate is processed chemically. The reconstruction is done in a different unit. The real image is digitized slice by slice, to capture the whole 3D information in an image stack.

Finally, the surface is determined numerically from the image volume. The final digital surface model is visualized as a 3D model (e.g. VRML).

6.2 Set up experiment

For the experiment, we searched for 25 probands with following characteristics:

- age range: between 18-23,
- Caucasian ethnics,
- no amalgam fillings,
- male-female ratio approx 1/1.

Before starting the experiments, we also described the physical morphology of the face, measured the Body Mass Index of all probands, and we took three photographs of the probands face: one frontal, one lateral, and one half profile.

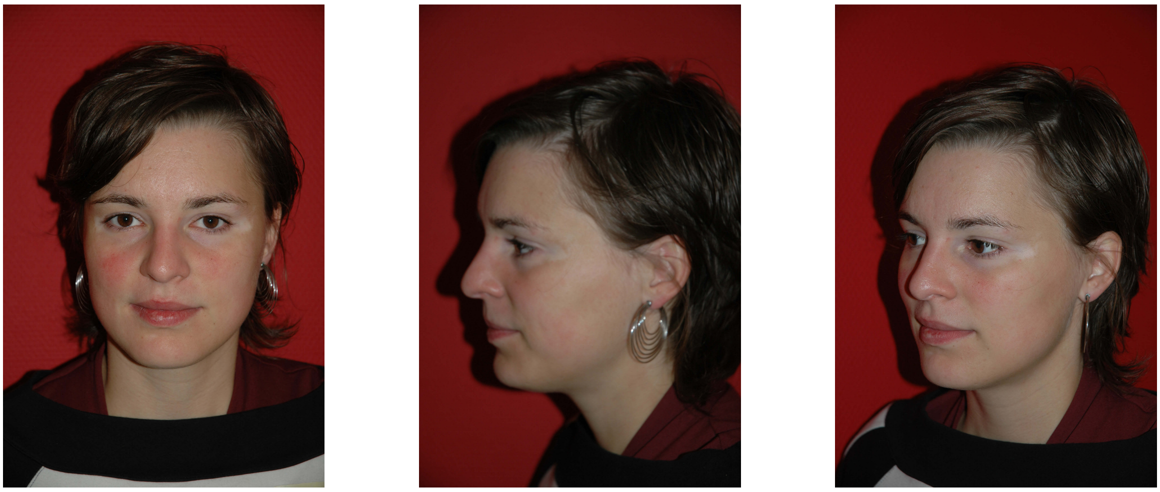

Figure 6.1: Photographs of the probands' face.
left: frontal, *middle:* lateral (profile), *right:* half profile.

We chose a small group of probands within a limited age range. Probands with dental amalgam fillings were excluded as these fillings provoke a scattering effect on CT (Computed Tomography) images. This would definitely influence the soft tissue measurements in the cheek area. Additionally, the dental scattering creates a lot of artefacts on the working model.

Different dental occlusions show different facial shapes e.g. a mandibular protrusion is typical for a class-III occlusion. In our experiment, all probands showed a class-I occlusion, in order to obtain a moderate facial outline.

Finally, we included 13 female and 12 male probands in the study. All probands received an 'informed consent', explaining the aim of the experiment and the recording technique of both holographic recording and low-dose Computed Tomography.

Probands were explained that they can stop contributing to the experiment at all times. They were also informed that participating in the experiment included no risk. Women who (thought they) were pregnant, giving breast-feeding, or could not show any adequate contraception method, were excluded from the experiment.

A face is recognisable from the hologram. Probands were guaranteed that all data were strictly investigated at CAESAR (center of advance European studies and research) in Bonn, and at the University of Düsseldorf.

Pictures of proband's faces and holographic surfaces could only be shown in scientific articles and presentations. Finally, probands received a small contribution fee. Both the low-dose CT and the hologram were taken at the University Hospital Gent, Belgium. For the convenience of the probands, both recordings were performed in one session.

6.3 Mobile holographic camera

A new mobile system was designed in cooperation with *Geola UAB*. The HSF-MINI has a compact design and can be used both on site and in laboratory. The main characteristics of this camera is its flexibility in time and space: the whole set up can be done in a short time, and the system can be transported in a little van. The camera also works in normal light conditions. A shutter is mounted on the mobile camera to make daylight recordings. For comparison, the holographic lab system works at red room light.

Figure 6.2: Mobile holographic unit HSF-MINI developed together with Geola Uab (Lithuania). The camera is shown without the diffuser plates for eyes-safe operation. The tower on the right houses (from top to bottom) the control unit, the laser power supply, the amplifier power supply and the cooling unit.

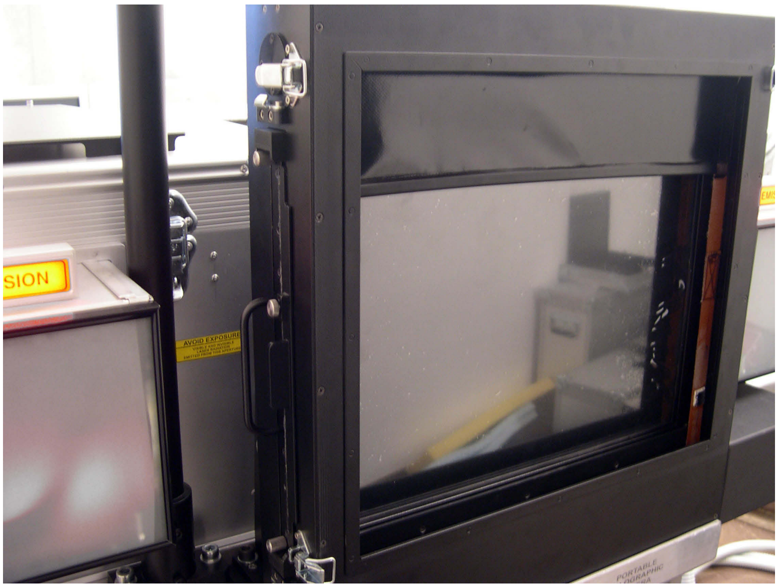

Figure 6.3: The curtain of the shutter exposes the holographic plate. The images show the state shortly after exposure.

The elements of the mobile holographic unit are the control unit, the beam delivery, the shutter system and the Nd:YAG laser.

The optical elements for beam forming and the laser are mounted on the same breadboard; so the breadboard space could be reduced to half the size.

The Nd:YAG laser in the mobile camera operates at a wavelength of 532 nm, instead of the 526.5 nm of the lab camera. Thus, the wavelength of the mobile unit matches precisely the read-out wavelength used during the optical reconstruction. The frequency doubled Nd:YAG laser is optimised for portrait holography. Recordings of the skin are possible due to the very short laser pulse in the green area.

The RIG for delivery of the reference beam is mounted on top of the camera, so the complete camera unit can be moved in one piece, which is an advantage in terms of the mobility of the holographic unit.

The lab system has a reference beam length of about 9 m; in contrast, the reference beam length of the mobile unit is reduced to approximately 3.60 m.

The beam is diverted inside the camera housing; one part is used for illumination, the other part is used as reference beam. The illumination part is again split up and directed to the left and right port. The reference beam is directed through an aperture on the upper side of the camera unit by a mirror inside the camera case. The beam arrives at the hologram plate over two external mirrors.

The illumination level for medical portrait holography is specified in the regulations for eye safety. The exposure limits for eye safe recordings are stricter than the exposure limits for skin. The cornea of the eye is exposed to pulsed laser radiation; the final energy density in the focus on the retina depends on wavelength, the eye geometry and the energy density. Laser light scattered by a diffuser is treated like an extended light source.

In traditional holography, working in darkness or under safe-light conditions is crucial. The mobile holographic unit includes a *shutter system* that allows daylight capturing of hologram up to a light intensity of about 300 lux. When the exposure is triggered, a curtain starts revolving around the holographic plate. The high energy pulse is synchronized to the moment when the shutter exposes the entire plate. Then the curtain rotates to its initial position. For this purpose, a cassette system was developed for inserting the holographic plate into the camera under normal light conditions. For hologram capture, a metal cover is retracted, and the holographic plate is only protected by the shutter curtain. After the recording, the metal sheet is inserted again, and the cassette can be removed safely.

The mobile holographic system is operated entirely by a single computer program, developed under the language LabWindows® (National Instruments), and runs under the operating system Windows 98. All parameters are set automatically at the system set up. The standard recording principle is simple.

In order to examine the effect of gravity on the facial soft tissue in our experiment, it was obvious we also had to take a holographic recording of the probands in lying position. The camera is then equipped with an additional mirror at a 45 degree angle above the lying proband to yield a frontal view. The additional mirror guides the illumination light to the person side, which is oriented away from the camera.

Figure 6.4: Mobile holographic unit. Positioning of the probands in upright (*left*) and reclined position (*right*).

6.4 Protocol low-dose CT

As already mentioned, both the CT and the holographic recording were performed at the same day. The main reason was to avoid changes in the soft tissue outline of the face, in order to create equal outlines both on CT and holographic surface, as these outlines are crucial in the regional registration step (chapter 6.2).

For recording the CT data, we used a 4-slices SIEMENS Somatom Plus. The radiation dose of the recording is reduced by a factor of 10 (low-dose CT) compared to a conventional CT. The radiation dose was ethically approved by the Ethical Committee of the University of Ghent.

We used the following protocol:

- Voltage: 120 kV
- mAs product: 50 mAs
- Rotation time 1 sec
- Collimation 1 mm
- Slice cut 1.25 mm
- Feed per rotation 4 mm
- Recon interval 0.6
- Kernel H20S (soft Kernel)
- Field of View (FOV): 240 mm

7 Methods

7.1 Introduction

In forensic facial soft tissue depth measurement, there is a strong need for a contact-free, optical measurement system. As mentioned earlier, there are some major problems and difficulties in traditional ways of measuring facial soft tissue thickness (see 3.3).

We introduced a new method for measuring soft tissue thickness, using low-dose CT and hologram tomography, in order to create a *facial soft tissue database*. We will demonstrate the principles of using a holographic and CT dataset for soft tissue thickness estimation with the software RapidForm® (INUS technologies).

It is the first time a technique is developed to do high precision facial soft tissue measurements, resulting in an endless number of measurement points.

7.2 Soft tissue measurement

A critical step is to register the holographic dataset to the skull, since they have no common regions. To solve this problem, the facial surface was also extracted from the CT data. CT scans are recorded in a reclined position, whereas holograms are taken in an upright position. This is why only regions with little soft tissue displacement (due to gravity) are considered for the registration between the holographic and the CT facial surface model. These regions are mainly the back of the nose and the lower forehead.

RapidForm® is a powerful full featured software for processing 3D scan data. RapidForm® converts data from any 3D scanning device (laser, white light, CT/MRI) into high quality polygon meshes or geometrically solid models.

Initially, the DICOM files are uploaded to RapidForm® and are segmented to mark the bone outline. The built-in RapidForm® algorithm can provide a satisfying segmentation, for the bone threshold we

Figure 7.1: Area for regional registration.

used the typical Hounsfield value of 1250 HU. Although this choice is fairly standard, the segmentation of low-dose CT data is still a point of discussion (see 8.1) and needs to be verified in the future.

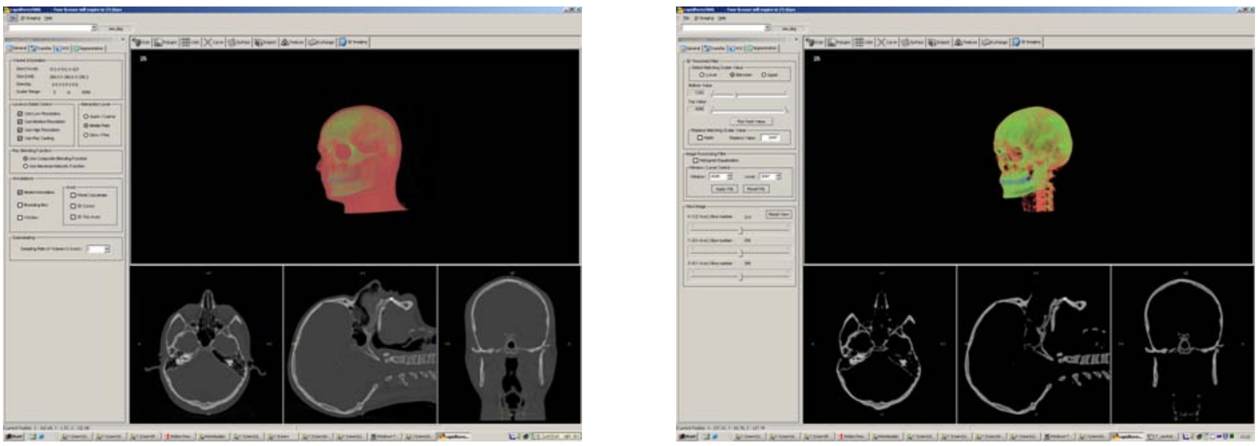

Figure 7.2: DICOM-files are uploaded to RapidForm®. *Left:* image with soft tissue outline. *Right:* image after segmentation.

From the volume data we created a polygonal isosurface. After eliminating stray points (scattering, ear fixation) we obtain a nice 3D working model of the skull. If necessary, we can derive a shell out of the polygonal isosurface. This allows us to significantly reduce the number of data, and retain only the surface of interest.

To mark the CT soft tissue outline it is necessary to perform another segmentation on the volume data. The second polygonal shell provides all the soft tissue information from the low-dose CT image. This polygonal shell will be the reference shell for positioning the holographic image. Via locking the

Figure 7.3: Polygonal isosurface, derived from the volume data of the low-dose CT (*left*), and a shell (*right*), used as a working model.

grid and performing consecutively both an initial and regional registration, we align both soft tissue outlines. The *initial* registration allows us to roughly adjust the images by picking reference points on both images. The first step is necessary to initialise the ICP algorithm (iterative closest point) based regional registration with a reasonable first guess.

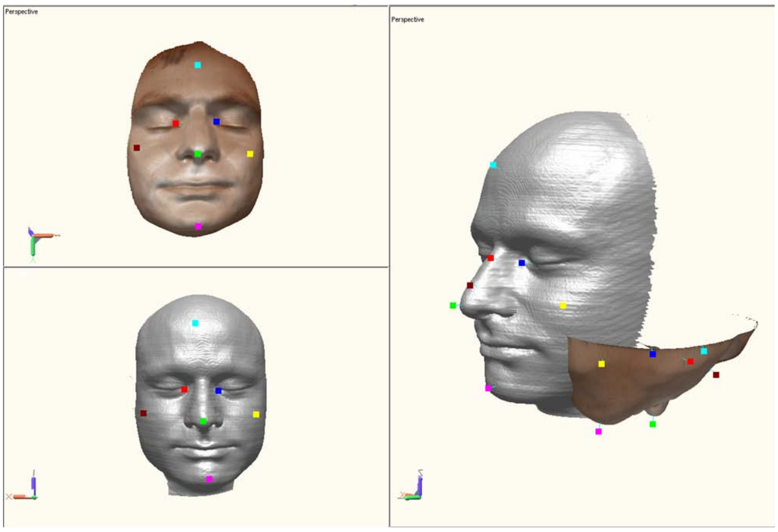

Figure 7.4: Inital registration between the soft tissue outline of the low-dose CT (*grey image*) and the holographic image (*brown*)

Using *regional registration*, we realize a precise superimposition of both the soft tissue polygonal shell and the holographic surface. After marking the region where we expect no soft tissue shift, superimposition of both shells will allow us to obtain a good positioning of the holographic surface to the polygonal shell of the skull.

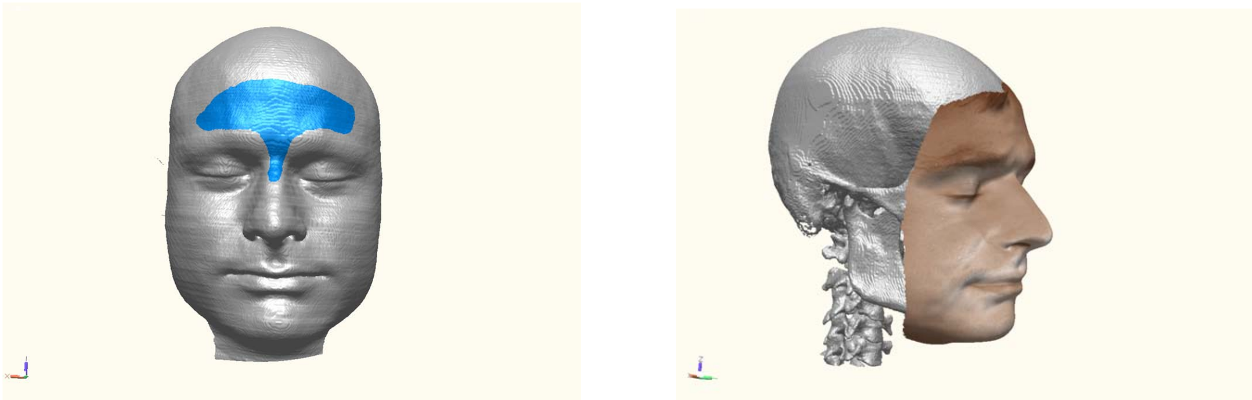

Figure 7.5: Regional registration, showing the area with no soft tissue shift (*left*), and superimposition of the holographic image over the skull (*right*).

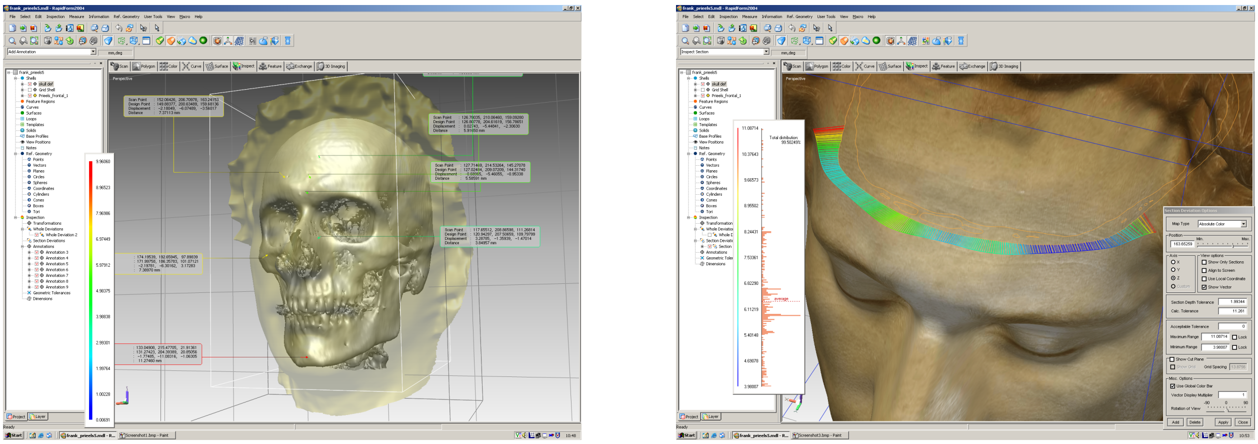

Figure 7.6: Visualization of the soft tissue thickness.

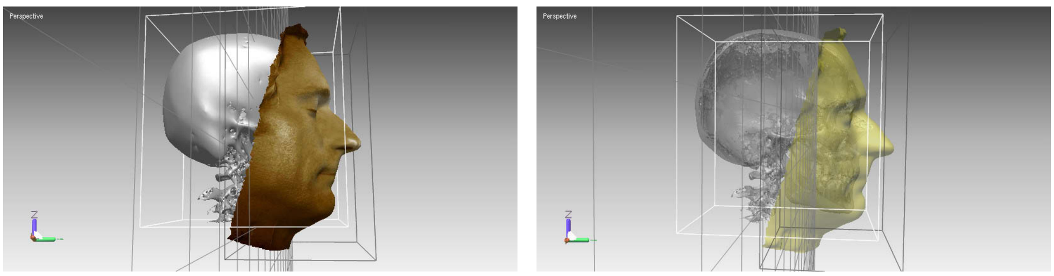

Figure 7.7: Visualization of the superimposition of holographic surface over the skull.

7.3 Reproducability of the technique

The soft tissue measuring technique was validated by showing the reproducibility of the technique. In a short interval of 15 minutes, 5 holographic recordings were taken of the same proband.

He was asked to keep the facial muscles relaxed, and to close the mouth in a gentle centric occlusion without any lip pressure. An occlusal centric relation is not indicated in these circumstances as it is very difficult to reproduce this position. A strong centric occlusal bite activates the musculus masseter, and thus creates a distortion in this area. Also a strong lip pressure can cause a soft tissue distortion.

A short time interval of holographic recordings is necessary in order to compare these 5 holographic surfaces in more or less identical situations. Holographic recordings taken over a longer time interval can lead to different facial outlines, due to fatigue, illness, short sleep, alcohol (swollen face) etc.

The holographic recordings in this validation test were performed on a fixed holographic unit at CAESAR in Bonn. This holographic unit has a wavelength of 526.5 nm. Compare to the mobile holographic system, which has a wavelength of 532 nm, it is necessary to use a correction factor. The correction over the three axes is about 1.1 %.

As these holograms were not used to make soft tissue measurements on the original CT image, it is clear that these results do not indicate the real soft tissue thickness. The only purpose is to compare the 5 holographic surfaces, both in matching one to another, and measuring the soft tissue layer.

All 5 facial shell surfaces were compared and generated in a distance map. Distance maps were colour coded. This showed these holograms were comparable.

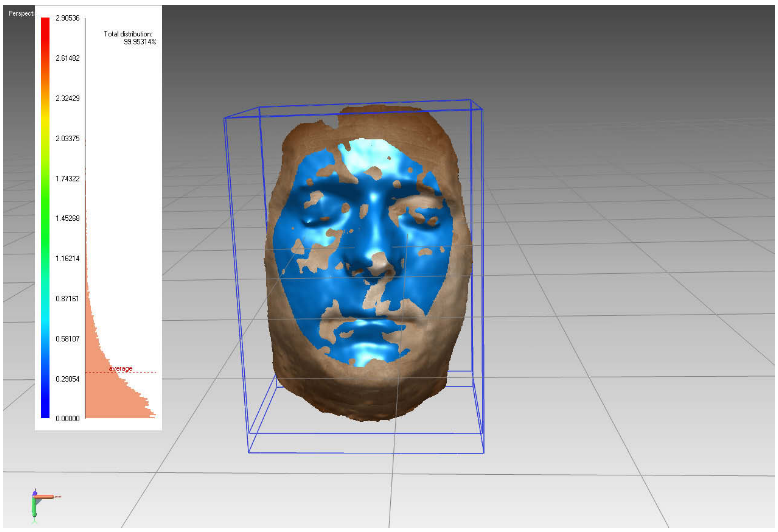

Figure 7.8: Superimposition of the holographic images, showing very small differences.

7.4 Results - evaluation

Using the procedure, as described in chapter 7.2, it is possible to create a soft tissue layer, wrapped over the skull. With the 'absolute colour' application in RapidForm®, the colour changes visualize the differences in soft tissue thickness.

The registration step between the holographic data and the soft tissue surface extracted from the CT data, is a critical step, as explained earlier. Due to this, two Helmer points (*nasion and glabella*) were chosen in the regional registration area. In that area the registration can be assumed to be correct, as to the minimal soft tissue shift due to the difference in positioning the proband when capturing the low-dose CT and the hologram. We also included a third Helmer point (*pogonion*) to show the accuracy of the registration in that area. We used the results of three probands for the comparison to the Helmer points. All three probands were male, with an average BMI.

The reason why we included only 3 Helmer points is just practical; it is not always that evident to mark the Helmer points on the skin. Due to the accuracy of the technique, it is difficult to mark one point on the skull. The diameter of an ultrasonic probe cannot be compared to the size of a voxel. We solved this problem by doing 5 measurements around the Helmer points (glabella, nasion, pogonion); the average thickness will be compared to the Helmer database.

When comparing these data, we have to keep in mind that Helmer used an ultrasound technique by positioning a sensor with a contact gel at the chosen anatomical landmarks; it has the disadvantage that the sensor is in direct contact with the the soft tissue, which might lead to deformations. The technique we used to measure the soft tissue thickness is contact free.

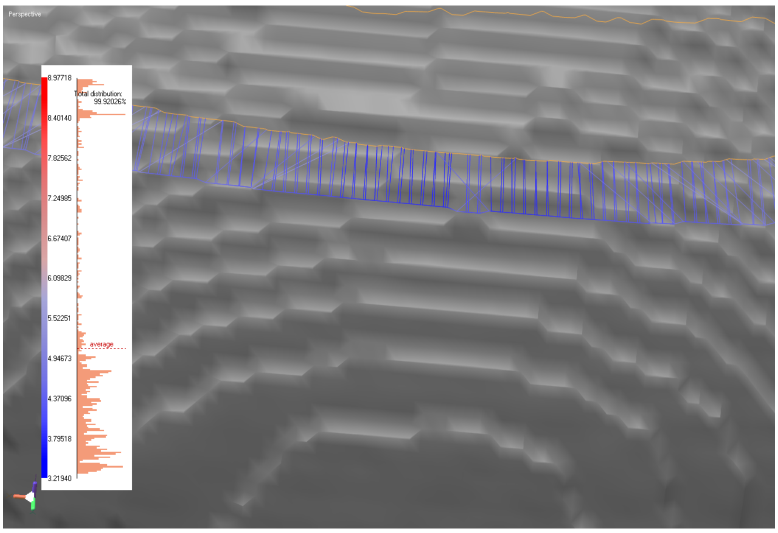

Figure 7.9: Possible measurement error due to the low resolution of the low-dose CT data.

Several error sources should also be considered, when comparing to the Helmer data:

- resolution of the CT data (fig. 7.9),
- localization of the Helmer points,
- regional registration between holographic and CT shells,
- statistical deviations due to the small number of probands.

Due to the large number of data, we used a sub-sampling ratio of 10 % ; this allowed us to handle the data easily.

Helmer found that the soft tissue thickness for different probands was not following a normal distribution. For this reason he used the median for characterization of the average value. He also stated a 95 % confidence interval for the values. In this age category (20-29 yrs old), Helmer took measurements on 13 male und 12 female probands. It is however remarkable that in some of his measurements, the mean is on the border of his 95 % confidence interval (table 7.1-3).
We calculated the mean and standard deviation of the 5 measurements on the 3 Helmer points. The standard deviation is an indication of the accuracy of the measurements. When comparing different data, considering on means and Standard deviations, we can conclude that - in most of the measurements - they fit within Helmer's 95 % confidence interval (table 7.4-6).

PROBAND 12 - 22 yrs old, female

Point 5	4.74	Helmer
(glabella)	4.75	mean 5.5
	4.66	VB (95 %) 5.0-5.5
	5.24	min 4.5
	4.99	max 6.3
mean	4.88	
std-dev	0.24	

Point 6	5.38	Helmer
(nasion)	5.31	mean 6.9
	5.39	VB (95 %) 6.0-7.0
	5.51	min 4.7
	5.50	max 7.3
mean	5.42	
std-dev	0.09	

Point 15	8.40	Helmer
(pogonion)	7.94	mean 9.6
	7.26	VB (95 %) 7.2-10.3
	8.61	min 6.7
	8.15	max 11.3
mean	8.07	
std-dev	0.52	

Table 7.1: Results of the measurements (in mm) at proband 12 on Helmer points 5, 6, 15.

PROBAND 16 - 21 yrs old, male

Point 5	5.23	Helmer
(glabella)	5.37	mean 5.7
	5.23	VB (95 %) 5.5-6.5
	5.47	min 5.2
	5.28	max 6.7
mean	5.32	
std-dev	0.10	

Point 6	6.54	Helmer
(nasion)	5.86	mean 8.2
	6.19	VB (95 %) 7.0-8.9
	5.79	min 6.3
	5.85	max 10.2
mean	6.05	
std-dev	0.32	

Point 15	11.07	Helmer
(pogonion)	11.23	mean 9.7
	10.24	VB (95 %) 8.2-10.2
	10.66	min 7.3
	10.03	max 13.7
mean	10.65	
std-dev	0.52	

Table 7.2: Results of the measurements (in mm) at proband 16 on Helmer points 5, 6, 15.

PROBAND 19 - 21 yrs old, male

Point 5	4.81	Helmer
(glabella)	4.53	mean 5.7
	4.70	VB (95 %) 5.5-6.5
	4.81	min 5.2
	4.81	max 6.7
mean	4.73	
std-dev	0.12	

Point 6	5.09	Helmer
(nasion)	5.10	mean 8.2
	5.08	VB (95 %) 7.0-8.9
	5.35	min 6.3
	5.52	max 10.2
mean	5.23	
std-dev	0.20	

Point 15	9.79	Helmer
(pogonion)	9.57	mean 9.7
	9.47	VB (95 %) 8.2-10.2
	9.41	min 7.3
	9.44	max 13.7
mean	9.54	
std-dev	0.15	

Table 7.3: Results of the measurements (in mm) at proband 19 on Helmer points 5, 6, 15.

PROBAND 12

Point 5	mean:	4.88
(glabella)	with std-dev	4.64-5.12
	Helmer 95 %	5.0-5.5

Point 6	mean:	5.42
(nasion)	with std-dev	5.33-5.51
	Helmer 95 %	6.0-7.0

Point 15	mean:	8.07
(pogonion)	with std-dev	7.55-8.59
	Helmer 95 %	7.2-10.3

Table 7.4: Comparing measurements (in mm) at proband 12 on Helmer points 5, 6, 15.

PROBAND 16

Point 5	mean:	5.32
(glabella)	with std-dev	5.22-5.42
	Helmer 95 %	5.5-6.5

Point 6	mean:	6.05
(nasion)	with std-dev	5.73-6.37
	Helmer 95 %	7.0-8.9

Point 15	mean:	10.65
(pogonion)	with std-dev	10.13-11.17
	Helmer 95 %	8.2-10.2

Table 7.5: Comparing measurements (in mm) at proband 16 on Helmer points 5, 6, 15.

PROBAND 19

Point 5	mean:	4.73
(glabella)	with std-dev	4.61-4.85
	Helmer 95 %	5.5-6.5

Point 6	mean:	5.23
(nasion)	with std-dev	5.03-5.43
	Helmer 95 %	7.0-8.9

Point 15	mean:	9.54
(pogonion)	with std-dev	9.39-9.69
	Helmer 95 %	8.2-10.2

Table 7.6: Comparing measurements (in mm) at proband 19 on Helmer points 5, 6, 15.

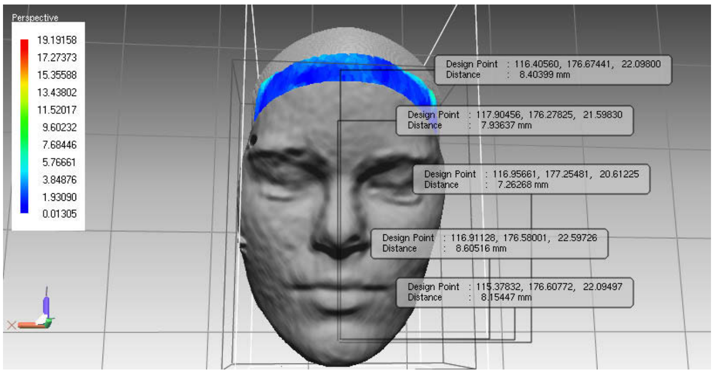

Figure 7.10: Screenshot proband 12, 5 measurements on Helmer point 15 (pogonion).

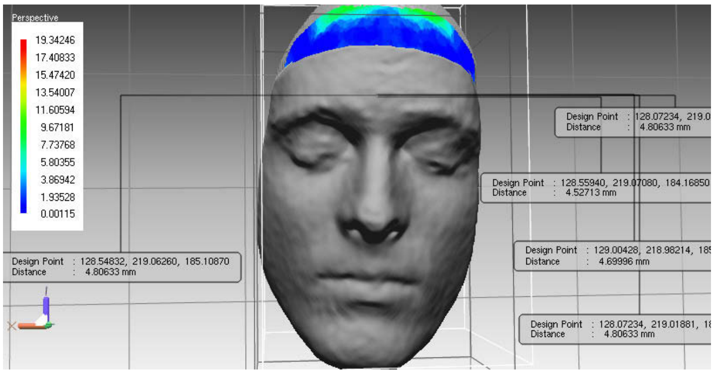

Figure 7.11: Screenshot proband 19, 5 measurements on Helmer point 5 (glabella).

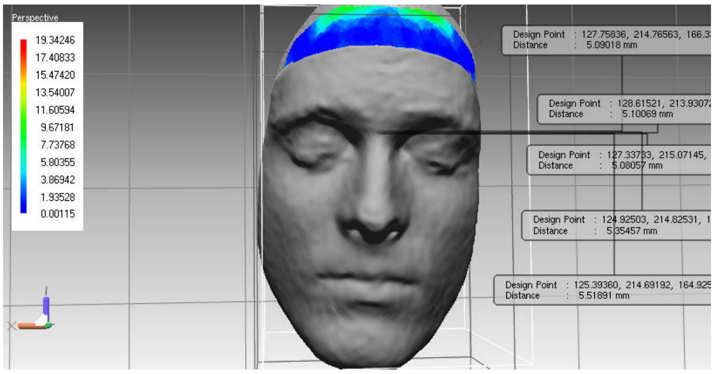

Figure 7.12: Screenshot proband 19, 5 measurements on Helmer point 6 (nasion).

8 Problems - considerations

8.1 Segmentation of low-dose CT data

Generally, a high radiation dose results in high-quality images. A lower dose leads to increased image noise and results in unsharp images.

The segmentation algorithm used in RapidForm® is a basic threshold segmentation on the Hounsfield values. A slide bar indicating the Hounsfield values , is used by the examiner; the segmentation can be checked immediately on the 3D-model. Due to the low-dose CT capturing, the segmentation is not optimal.

De Bock et. al. [SE1] developed a fast and memory efficient streaming framework for low-level segmentation of 3D volumes. Processing speed, reduced memory usage a streaming interface are desirable or a necessity in many applications. When segmenting using the traditional low-level segmentation algorithms, a large amount of memory is necessary.

The connected components problem for very large volumes was solved by splitting up the volume in multiple sub-volumes; the objects in each sub-volume were separately labelled with a standard sequential connected components labelling algorithm , checking the interconnections along the common border between neighbouring sub-volumes. Finally, the objects in the sub-volumes were relabelled according to the interconnections. This will reduce the memory usage.

Yan Kang et. al. [SE2] developed a highly automated three-dimensionally based method for the segmentation of bone in volumetric computed tomography datasets. They used a multistep approach starting with local adaptive thresholds, followed by procedures to correct boundary discontinuities and an anatomically oriented boundary adjustment using local values of cortical bone density. The comparison between these algorithms and the algorithms based upon a threshold segmentation of the Hounsfield values can be an interesting topic on further research.

8.2 Soft tissue shift

The expression of the face is strongly determined by the effect of gravity on the skull and the soft tissue. Both the skull and the skin outline are well described; the effect of internal and external forces is difficult to investigate.

The effect of gravity on the facial soft tissue can be demonstrated by comparing the visual appearance of a person in an upright and reclined position.

Figure 8.1: Two digital photographs taken with the same distance and same focal length, to show the difference between an upright (*left*) and reclined (*right*) position.

Figure 8.2: Soft tissue shift between upright and reclined position, lateral (*left*) and frontal (*right*) view.

In medical applications such as plastic surgery and forensic science, the interaction between a reclined and an upright face is relevant for the appearance of the face. The visual appearance of a face is in an upright position, but both recordings of CT scans and performing surgery is in a reclined position.

We conduct an experiment to quantify the deformation of the facial soft tissue between upright and reclined position. We need unique reference features on the face and a common reference on the skull, meaning it is fixed to the underlying bone structure, and without any possible influence of gravity.

For this experiment, we fabricated an interocclusal jig as a fixed reference device. Impressions were taken from the test person's upper and lower dental arch, together with an occlusal bite registration in centric relation. The test person was asked to bite in central occlusion; due to the minimal thickness of the jig of about 2 mm, we ended in an occlusal centric relation. This was of no importance since we only wanted to create a fixed reference platform to visualise the facial soft tissue shift.

Figure 8.3: The jig adapted to the proband bite, with 4 white marker points and small holes of 200 µm inside.

The purpose of the jig is to carry 4 defined marker points that can be visualised in the reconstructed image. For this, impressions were taken from the upper and lower jaw of the proband. We fixed metal wires into the hard resin jig; these wires extended outside the mouth towards the lateral sides of the face. The wires fork at the end, where 2 marker points are attached at each side; a special reflective foil (diameter 5 mm) is attached to the fork's end, penetrated by a very small hole of 200 µm. These holes are the reference points in the real image.

In this experiment, 2 holographic recordings are performed, one in upright and one in reclined position.

The 4 reference points are visualised as red spheres on the models.
The measurements of the models are performed with RapidForm®.
Comparison between the two surfaces is the next step. Skin features or special marks are identified

Figure 8.4: Set-up for upright and reclined topometry. The proband wears the jig in each recording.

in both models; the shift between these points is calculated. When moving from sitting to reclined position, there is a soft tissue shift upwards and outwards.

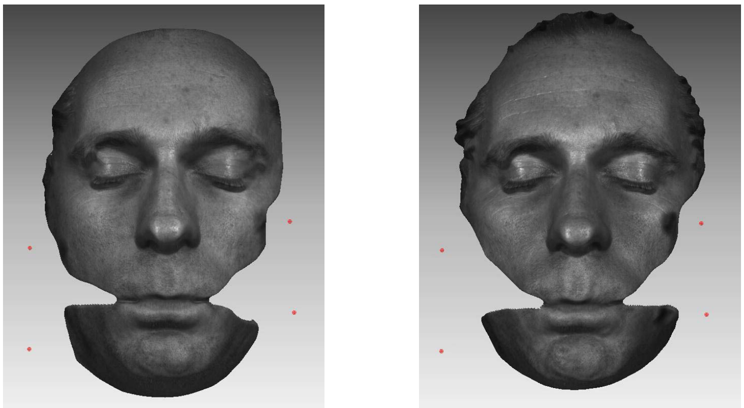

Figure 8.5: The captures resulted in two digital models of the proband, one in reclined (*left*) and one in upright position (*right*). The red balls are the identified marker points. Both cheeks are missing in these surface models, since these regions were strongly affected by artefacts from the wires suspending the marker points.

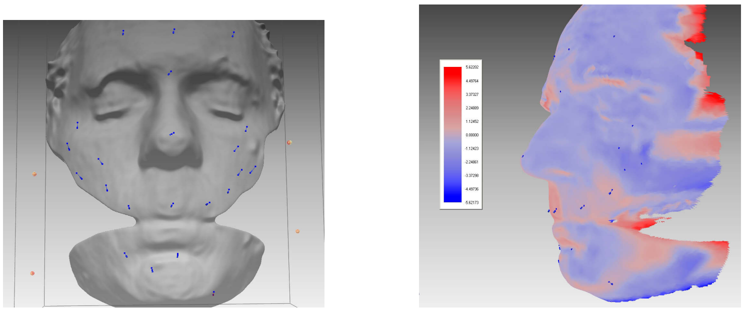

Figure 8.6: Perspective of the face model, showing the displacement (*left*), a colour coded difference map from comparing the upright and the reclined face model volumetrically (*right*).

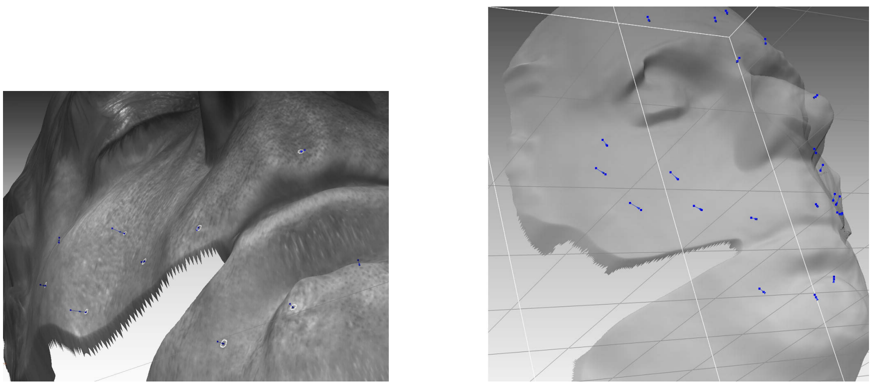

Figure 8.7: Close-up (*left*) and general perspective (*right*), showing the displacement vectors.

8.3 Tilted image

While matching low-dose CT and holographic data, 2 problems occurred.

During the regional registration step, the holographic image is superimposed to the soft tissue outline of the low-dose CT image. Due to gravity, comparable areas can only be found in the upper part of the face. This also means there are no matching areas in the lower part of the face. Due to this discrepancy, there is a risk of an image shift in the horizontal plane. The solution to the problem was to enlarge the area of regional registration.

When comparing the 5 holographic surfaces in the validation test, another image shift occurred. As both the soft tissue outline of the low-dose CT image and the holographic surface outline crossed each other in a vertical plane, we use the term 'tilted image'.

As all 5 superimpositions showed the same tilted image, it was clear that it was not a holographic capture problem. Due to the manual built up of the scanning system, the laser beam did not rectangularly section the scanner plate. A new, fixed scanner solved the problem of the tilted image [Ho-In9].

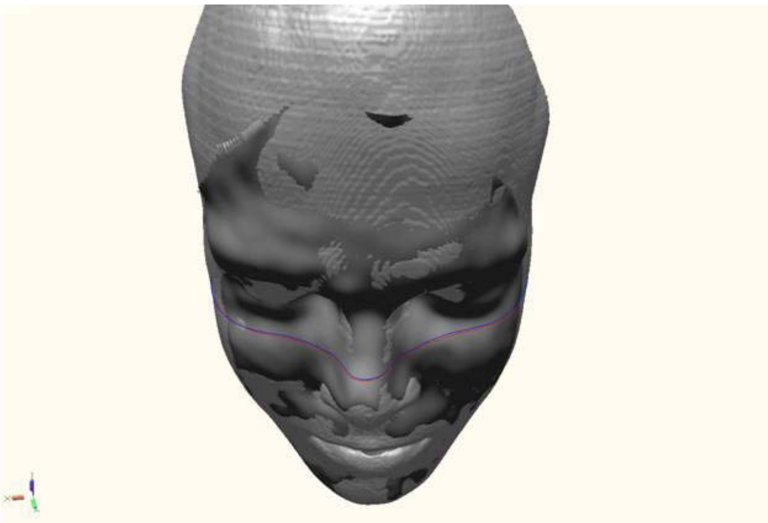

Figure 8.8: Horizontal slice, showing the tilted images, due to a lack of matching areas in the lower part of the face.

9 Conclusion

Summary

For many years, there is a need for an accurate database on facial soft tissue thickness, using a contact-free optical measurement system. All previous techniques were not adequate, due to both the measuring technique and the limited number of facial measuring points.

We introduced a new technique, using information from both low-dose CT and holography. The use of low-dose CT allowed us to reduce the radiation significantly compared to the conventional CT. The radiation dose was ethically approved by the Ethics Committee of the University of Ghent. Holography was the perfect tool to create a highly detailed facial outline. In the Holography and Laser Technology Group (Prof. Hering) at the CAESAR foundation in Bonn, the use of analog portrait holography was introduced as a tool for facial topometry, using a short-pulsed green laser.

In a first step, the technique of measuring facial soft tissue thickness by comparing holographic and low-dose CT data was validated at CAESAR in Bonn. In a short interval, five holographic recordings were taken of the same proband. All five facial shell surfaces were compared, distance maps showed that these recordings were close to identical.

A mobile holographic unit realized the holographic capture of the probands at the University Hospital in Ghent (Belgium). The camera can be set up quickly and is able to capture holograms in daylight conditions.

A critical step was to register the holographic dataset to the skull, since they have no common regions. To solve this problem, the facial surface was also extracted from the CT data. CT scans are recorded in a reclined position, whereas holograms are taken in an upright position. This is why only regions with little soft tissue displacement were considered for the registration between the holographic and the CT facial surface model. For the evaluation of the measurements, we compared our results on three points on the skull surface (as defined by Prof. Helmer) with the actual database established by Prof. Helmer, taking into account that the accuracy of both measuring techniques is completely different.
Finally we discussed the segmentation of low-dose CT data, and the soft tissue shift between an upright and a reclined position.
It is the first time a technique is developed to do high precision facial measurements.

Perspectives

Using our method, it is possible to create a soft tissue layer, wrapped over the skull. Due to the fact that these measurements are very precise, the technique can be used in facial forensic reconstruction, but also in maxillofacial plastic surgery.

The scope of this thesis was to make a proof of concept in measuring facial soft tissue. Enlarging the number of probands and dividing them in subcategories will be necessary to create a reliable database on facial soft tissue thickness.

Further research on the soft tissue shift can open perspectives in using CT data, available in hospital databases.

The evolution in digital holography, in combination with our technique can be used in forensic sciences to clearly show the soft tissue changes during biting (bite marks) in crime cases.

Bibliography

[FR1] PX Iten, Identification of skulls by video superimposition. *J. Forensic Sci.*, 32 (1987) 173-188.

[FR2] S. Seta and M. Yoshino, a combined apparatus for photographic and video superimposition. In M.Y. Iscan and R.P. Helmer (eds.), *From the Bare Bone to the Full Face*, Wiley-Liss, New York, 1993, pp161-169.

[FR4] G.J.R. Maat, The positioning and magnification of faces and skulls for photographic superimposition, *Forensic Sci. Int.*, 41 (1989) 225-235.

[FR5] F.B. Cocks, The Barkly Highway murder., *Aust. Pol. J.*, 24 (1970) 173-185

[FR6] K.A. Brown, Developments in cranio-facial superimposition for identification., *J. Forensic Odontostomatol.*, 1 (1983) 57-64

[FR7] R.P. Helmer, J.B. Schimmler and J. Rieger, On the conclusiveness od skull identification via the video superimposition technique, *J. Can. Soc. Forensic Sci.*, 2 (1989b) 177-194

[FR8] T. De Vore, Radiology and photography in forensic dentistry., *Dent. Clin. North Am.*, 1977 Cited by Nichersen et al.

[FR9] K. Brown, B. Clarke, C. Hollamby, I. Congdon, Identification in the Truro murders. Presented at the *7th Australian International Symposium on the Forensic sciences*, Sydney, 1981. Cited by Nichersen et al.

[FR10] R.A.H. Neave, Pictures in the round: Moulage and models in medicine. *J.Audiovis. Media Med.*,12 (1989) 80-84.

[FR11] B.P. Gatliff, Facial sculpture on the skull for identification, *Am. J. Forensic Med. Path.* 5 (1984) 327-356.

[FR12] M.M. Gerasimow, The face finder. New York: Hutchinson (1971).

[FR13] K. Taylor, Forensic art and illustration. Boca Raton: CRC Press (2001).

[FR14] G. Hodson, L.S. Lieberman, P. Wright, In vivo measurements of facial soft tissue thickness in American Caucasoid children, *J. Forensic Sci.*, 30 (1985) 1110-1112.

[FR15] P.C. Caldwell, New questions (and some answers) on the facial reproduction techniques. In: K.J. Reichs (Ed), Forensic Osteology. Charles C. Thomas, Springfield, 1986, pp. 229-254.

[FR16] E.R. Dumont, Mid-facial depths of white children; an aid in facial reconstruction, *J. Forensic Sci.*, 31 (1986) 1463-1469.

[RE1] V. Bruce and A. Young, Understanding Face Recognition. *British Journal of Psychology 77* (1986) 305-27.

[RE2] J. Shepherd, Social factors in face recognition. In G. Davies, H. Ellis, and J. Shepherd (eds.). *Perceiving and Remembering Faces*, London: Academic Press.

[RE3] C. Wilkinson, Forensic Facial Reconstruction. Cambridge University Press 2004.

[RE4] S.J. Mc Kelvie, Sex differences in facial memory. In M.M. Gruneburg, P.E. Morris and R.N. Sykes (eds.), *Practical Aspects of Memory.* London: Academic Press, pp 263-9.

[HI1] H. Welcker, Zur kritik des Schiller's Schädel, *Arch. Anthropol.* 17 (1888) 19-60.

[HI2] H. Welcker, Der Schädel Dante's, *Jahrbuch der Deutschen Dante-Gesellschaft*, Vol. 1. Leipzig, 1867.

[HI3] H. Welcker, Schiller's Schädel und Todenmaske, nebst Mitteilungen uber Schädel und Todenmaske Kants. Fr. Vieweg und sohn, Braunschweig, 1883.

[HI4] W. His, Anatomische Forschungen über Johann Sebastian Bach's Gebeine und Antlitz nebst Bemerkungen über dessen Bilder. Abhandlungen der Mathematisch-Physikalischen Klasse der Königlichen, Sächsischen Gesellschaft der Wissenschaften, 22 (1895) 379-420.

[HI5] W.M. Kollmann, W. Büchly, Die perzistenz der rassen und die reconstruction der physiognomie praehistorischer Schädel, *Arch. Anthopol.* 25 (1898) 329-359.

[2D1] D.G. Cherry, J.L. Angel, Personality Reconstruction from Unidentified Remains, *FBI Law Enforcement Bulletin* 48 (1977) 12-15.

[2D2] W.M. Krogman, M.Y. Iscan (1986), *The human skeleton in forensic medicine.* (2^e) Springfield, Thomas.

[2D3] R.M. George, The lateral craniographic method of facial reconstruction. *J. For. Sci.* 32 (1987), 5, 1305-30.

[2D4] D.H. Ubelaker, *Human Skeletal Remains: Excavation, Analysis, Interpretation, Manuals of Archaeology.* (2^e). Washington DC, Smithsonian Institute Press (1978).

[2D5] D.H. Ubelaker, G. O4Donnell, Computer-assisted facial reproduction. *J. For. Sci.* 37 (1992) 155-62.

[STM1] J. Czekanowski, Untersuchungen über das Verhältnis der Kopfmasse zu den Schädelmassen. *Archiv für Anthropologie* 34 (1907), 42-89.

[STM2] D. Berger, Untersuchungen über die Weichteildickenmasse des Gesichts. Frankfurt/Main: Diss (1965).

[STM3] D. Leopold, Identification durch Schädeluntersuchung unter besonderer Berücksichtigung der Superprojection. Leipzig: Habilitationsschrift (1968).

[STM4] K. Suzuki, On the thickness of the soft parts of the Japanese face. *Journal of Anthropology ot the Society ot the Nippon* 60 (1948), 7-11.

[STM5] J.S. Rhine, H.R. Campbell, Thickness of facial tissues in American Blacks. *J. Forensic Sci.*,25 (1980), 4, 847-58.

[STM6] J.S. Rhine, C.E. Moore, J.T. Westin (eds.) Facial Reproduction: Tables of Facial Tissue Thickness of American Caucasoids in Forensic Anthropology. Maxwell Museum, technical Series, n°1, University of New Mexico (1982).

[STM7] I.M. Bankowski, Die Bedeutung der Unterkieferform und -stellung für die Photographische Schädelidentifizierung. Diss., Frankfurt (1958).

[STM8] W. Weining, Röntgenologische Untersuchungen zur Bestimmung der Weichteildickenmasse des Gesichts. Dissertation, Frankfurt (1958).

[STM9] W.A. Aulsebrook, P.J. Becker, M.Y. Iscan, Facial soft tissue thickness in the adult male Zulu. *Forensic Science International* 79 (1996) 83-102.

[STM10] V.M. Phillips, N.A. Smuts, Facial reconstruction; utilidation of computerised tomography to measure facial tissue thickness in a mixed population. *Forensic Science International* 83 (1996), 51-9.

[STM11] D. Sahni, Preliminary study on facial soft tissue thickness by magnetic resonance imaging in Northwest Indians. *Forensic Science Communications* 4 (2002), 1.

[STM12] R. Helmer, Schädelidentifizierung durch elektronische Bildmischung. Heidelberg, Kriminalistik-Verlag (1984).

[STM13] G.U. Lebedenskaya, T.S. Balueva, E.B. Veselovskaya, Development of methodological principles for reconstruction of the face on the basis of skull material. In M.Y. Iscan and R.P. Helmer (eds.), Forensic Analysis of the skull. New York: Wiley-Liss Inc., pp. 183-98 (1993).

[STM14] S. De Greef et. al, Semi-automated ultrasound facial soft tissue depth registration: method and validation. *J. Forensic Sci.*, 50 (2005).

[Ho-In1] M.A. Papadopoulos, P.K. Christou, A.E. Athonasiou, P. Boettcher, H.F. Zeilhofer, R. Sader, N.A. Papadopulos. Three-dimensional craniofacial reconstruction imaging. *Oral Surgery, Oral Medecine, Oral Pathology, Oral Pathology*, 93:382-393 (2002).

[Ho-In2] F. Chen, G.M. Brown, M. Song, Overview of three-dimensional shape measurement using optical methods. *Optical Engineering*, 39: 10-22 (2000).

[Ho-In3] J. Bongartz, D. Giel, S. Frey, A. Thelen, P. Hering. Hochauflösende dreidimensionale Gesichtsprofilvermessung mit kurzgepulster Holographie. *Physikalische Methoden der Laser und Medizintechnik*, pages 51-56. VDI Verlag (2003).

[Ho-In4] J. Bongartz, *Hochauflösende dreidimensionale Gesichtsprofilvermessung mit kurtzgepulster Holographie.* PhD thesis, Mathematisch-Naturwissenschaftliche Fakultät der Heinrich- Heine-Universität Düsseldorf (2002). *http://docserv.uni-duesseldorf.de/servlets/DocumentServlet?id=2192*

[Ho-In5] D. Gabor, A new microscopic principle. *Nature*,161: 777-778 (1948).

[Ho-In6] D. Giel, *Hologram Tomography for Surface Topometry.* PhD thesis, Mathematisch-Naturwissenschaftliche Fakultät der Heinrich-Heine-Universität Düsseldorf (2003). *http://docserv.uni-duesseldorf.de/servlets/DocumentServlet?id=2598*

[Ho-In7] S. Frey, *Three-dimensional facial measurement by portrait holography and texture-based focus detection.* PhD thesis, Mathematisc-Naturwissenschaftliche Fakultät der Heinrich-Heine-Universität Düsseldorf (2005). *http://docserv.uni-duesseldorf.de/servlets/DocumentServlet?id=3166*

[Ho-In8] A. Thelen, *Optimized surface extraction from holographic data.* PhD thesis, Mathematisch-Naturwissenschafliche Fakultät der Heinrich-Heine-Universität Düsseldorf (2006). *http://docserv.uni-duesseldorf.de/servlets/DocumentServlet?id=3430*

[Ho-In9] S. Hirsch, *Digital and Analog Hologram Tomography for Medical Applications.* PhD thesis, Mathematisch-Naturwissenschaftliche Fakultät der Heinrich-Heine-Universität Düsseldorf (2006).

[Ho-Pr1] P. Hariharan, *Optical Holography. Principles, Techniques and Applications.* Cambridge University Press (1996).

[Ch-Pr1] H.I. Bjeklhagen, *Silver-Halide Recording Materials for Holography and Their Processing.* Springer-Verlag, Berlin Heidelberg New-York (1995).

[Ch-Pr2] N. Ladriere. Optische und chemische Aspekte der hochauflösenden, vollautomatischen Hologramentwicklung. Master's thesis, Fachbereich Photoingenierwesen und Medientechnik an der Fachhochschule Köln, 2004.

[Ch-Pr3] N. Ladriere, S. Frey, A. Thelen, S. Hirsch, J. Bongartz, D. Giel, P. Hering. Ultraschnelle holographische Gesichtsprofilvermessung mit vollautomatischer Hologramentwicklung. In Hartmann, Kohl-Bareis, Hering, Lonsdale, Bongartz und Buzug, editors, *"Aktuelle Methoden der Laser-und Medizintechnik"*, pages 272-274. VDE-Verlag, 2004.

[SK1] T.D. Stewart, Medicolegal aspects of the skeleton: age, sex, race and stature. *American Journal of Physical Anthropology 6* (1948): 315-21.

[SK2] T.D. White, P.A. Folkens, *Human Osteology.* San Diego: Academic Press Inc. (1991).

[SK3] R. Helmer, Y. Iscan, Assessment of the reliability of facial reconstruction. In Iscan and Helmer, 1993, pp 229-47.

[SK4] N.J. Sauer, Forensic Anthropology and the concept of race - if races don't exist, why are forensic anthropologists so good at identifying them? *Social Science and Medicine* 34, 2 (1992), 107-11.

[SK5] D.R. Brothwell, *Digging up bones.* British Museum: Cornell University Press (1981).

[SK6] D.H. Enlow, *Handbook of Facial Growth.* Philadelphia PA: W.B. Saunders (1982).

[CT1] W.A. Kalender: *Computed Tomography. Fundamentals, System Technology, Image Quality, Applications.* Publicis MCD Verlag (2000).

[CT2] R.A. Brooks: Principles of computer assisted tomography (CAT) in in radiographic and radioisotopic imaging. *Phys. Med. Biol.* 21: 689-732 (1976).

[CT3] H.J. Scudder: Introduction to computer aided tomography. Proceedings of the IEEE; 66 (6): 628-637 (1978).

[CT4] H. Morneburg (Ed.): *Bildgebende Systeme für die medizinische Diagnostik.* München: Publicis MCD (1995).

[CT5] W.A. Kalender, A. Polacin, C. Süss: A comparison of conventional and spiral CT: an experimental study on the detection of spherical lesions. *J. Comp. Assist. Tomogr.*, 18: 167-176 (1994).

[SE1] J. De Bock, W. Philips: A fast and memory efficient streaming framework for low-level segmentation of 3D volumes.

[SE2] Yan Kang, K. Engelke, W.A. Kalender: a new accurate and precise 3D segmentation method for skeletal structures in volumetric CT data. *Medical Imaging, IEEE transactions on* 22 (5): 586-598 (2003).

[OR1] J.N. Latta: Computer-based analysis of hologram imagery and aberrations. I. holographic surface types and their nonchromatic aberrations. *Applied Optics*, 10 (3): 588-608 (1971).

[OR2] VRML 97. The virtual reality modelling language: ISO / IEC 14772-1: 1997, *http://www.web3d.org/X3d/specifications/vrml/*

Acknowledgements

I would like to thank all the people who were involved in the holographic project, and gave support for this thesis.

First of all, I would like to thank Prof. Dr. Peter Hering for the opportunity to join his holography group, his strong support and his trust in my abilities.

I also want to thank Prof. Dr. Stefanie Ritz-Timme for accepting the second referee of this work.

The collaboration with Dr. Andrea Thelen was very fruitful; especially the amount of time and patience she spent in introducing me into 3D graphics and holography.

My good collegue and friend Dr. Sven Hirsch I thank for the critical support, the intensive brainstorming, the late hours in the lab... and the nice friendship.

From the coworkers in the holography group, I want to thank Nicola Gisbert for the help during the finishing of the lab work, and also Philipp Seidel.

I gratefully thank Prof. Dr. Rik Achten (Medical Imaging, University of Ghent, Belgium) for proposing to host CT and holography capturing at his department. I appreciate his support and believe in the project.

I would like to thank my parents for all the opportunities I got.

A special thank to Lieve and Marie.

And to Marja, for an unspoken support and a wordless understanding.

And finally, to my boys Gijs and Bregt, for their blind faith in all my projects. They are my true companions. That it may last.